PIPE: Physics-Informed Position Encoding for Alignment of Satellite Images and Time Series in Typhoon Forecasting

Haobo Li[1] **Eunseo Jung**[1] **Zixin Chen**[1] **Zhaowei Wang**[1]
Yueya Wang[2] **Huamin Qu**[1] **Alexis Kai Hon Lau**[2]
[1] Department of Computer Science & Engineering
[2] Division of Environment & Sustainability
Hong Kong University of Science and Technology
hliem@connect.ust.hk

Abstract

Multimodal time series forecasting is foundational in various fields, such as utilizing satellite imagery and numerical data for predicting typhoons in climate science. However, existing multimodal approaches primarily focus on utilizing text data to help time series forecasting, leaving the visual data in existing time series datasets underexplored. Furthermore, it is challenging for models to effectively capture the physical information embedded in visual data, such as satellite imagery's temporal and geospatial context, which extends beyond images themselves. To address this gap, we propose **p**hysics-**i**nformed **p**ositional **e**ncoding (**PIPE**), a lightweight method that embeds physical information into vision language models (VLMs). **PIPE** introduces two key innovations: (1) a physics-informed positional indexing scheme for mapping physics to positional IDs, and (2) a variant-frequency positional encoding mechanism for encoding frequency information of physical variables and sequential order of tokens within the embedding space. By preserving both the physical information and sequential order information, **PIPE** significantly improves multimodal alignment and forecasting accuracy. Through the experiments on the most representative and the largest open-sourced satellite image dataset, **PIPE** achieves state-of-the-art performance in both deep learning forecasting and climate domain methods, demonstrating superiority across benchmarks, including a 12% improvement in typhoon intensity forecasting over prior works.

1 Introduction

Time series forecasting plays a crucial role in climate modeling [58]. This task involves modeling temporal dependencies to predict future values of a target variable, a challenge exacerbated by noise, non-stationarity, and the frequent need to integrate heterogeneous auxiliary data. While traditional methods like Autoregressive Integrated Moving Average (ARIMA) rely on statistical priors [12], deep learning architectures (e.g., LSTMs [13], Transformers [47]) have recently dominated the field by learning latent temporal patterns from data. However, these methods still struggle to deliver precise forecasts amid the complexity and scale of real-world data, leaving high-stakes tasks such as typhoon-track prediction continue to have a long way to go.

The rise of large language models (LLMs) as a type of sequence modeling has introduced new opportunities for time series forecasting. Although LLMs were originally built for NLP tasks such as text generation [36] and summarization [7], their core objective naturally aligns with time-series

39th Conference on Neural Information Processing Systems (NeurIPS 2025).

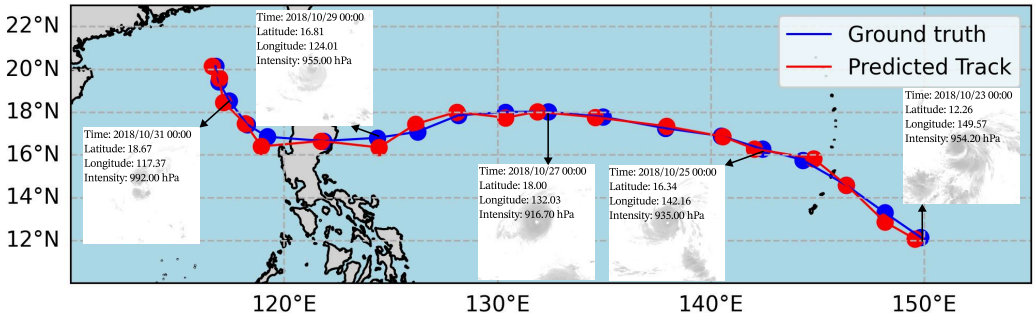

Figure 1: The multimodal time series forecasting task and the forecasting results for Typhoon Yutu by our PIPE-3B. The leading time is 12 hours and the time gap between neighbouring dots is 12 hours. In multimodal time series forecasting, satellite images can improve the forecasting accuracy.

forecasting: predicting the next token in a sentence mirrors forecasting the next value in a sequence, both conditioned on historical context. Consequently, existing work adapts LLMs to forecasting through tokenization techniques or patching technology to splice time-series segments into model context [62]. More recent work broadens the paradigm by injecting auxiliary instructions or descriptions through zero-/few-shot inference [4], in-context learning [32], and text-augmented forecasting [17]. Several studies push the scope further by incorporating explicit temporal cues, for example, TimeLLM [17] and UniTime [29] involve temporal information in prefix-prompts, while AutoTimes embeds timestamps as positional encodings to integrate the temporal information [32].

However, existing methods for multimodal time series forecasting, which integrate visual and numerical data, face numerous limitations. Integrating visual context, such as satellite imagery, into forecasting is indispensable in climate [48] and other domains [15, 52], yet state-of-the-art vision–language models (VLMs) like GPT-4o [36], Gemini [46], and Qwen-VL [2] are tuned primarily for general domain multimodal data. Furthermore, their projection layers, the vision encoder from CLIP [41], cross-attention [27], Q-Former [24], and MLP [28], solely focus on pixel-level semantics and overlook the rich physical metadata (e.g., timestamps and geo-coordinates) embedded in real-world imagery. This omission limits their capacity to improve high-stakes multimodal forecasting tasks. For example, typhoon track prediction with satellite imagery (Figure 1) requires correlating pixel values with the time-specific geophysical attributes (e.g., latitude, longitude) embedded in each pixel. As a result, addressing these overlooked physical dimensions beyond the pixel-level values in multimodal time-series forecasting not only fills a critical gap in existing alignment methods that only focus on the pixel-level values but also introduces a new task for multimodal alignment.

To address these challenges, we propose **p**hysics-**i**nformed **p**ositional **e**ncoding (**PIPE**), a lightweight method to embed latent physical metadata (e.g., timestamps, geospatial coordinates) into positional encodings. Unlike traditional positional encodings, which focus solely on the sequence order of tokens within one input instance [47, 11], **PIPE** encodes shared global physical knowledge (e.g., latitude-longitude relationships consistent across instances) while preserving sequence order information. Specifically, **PIPE** introduces two key innovations: (1) a physics-informed positional indexing scheme that maps physics to positional IDs, and (2) variant-frequency positional encoding that integrates the attributes of physical variables in the input embedding space. They maintain the original token topology while enabling explicit modeling of geographic-temporal dependencies. Experiments on the most representative and the largest open-sourced satellite image dataset for typhoons, Digital Typhoon [22], demonstrate improved cross-modal integration and forecasting accuracy. **PIPE** achieves state-of-the-art performance compared to general AI and domain models across multiple benchmarks on the multimodal time series forecasting task.

Our contributions are threefold:

- We propose the multimodal time-series forecasting scheme to integrate visual information, where time series data is accompanied by corresponding vision data, extending beyond conventional univariate/multivariate time series forecasting.

- We propose the **PIPE**[1], a method to embed physical knowledge into VLMs. Our method contains two key innovations: (1) physics-informed positional indexing and (2) variant-frequency positional encoding.
- Through comprehensive experiments on the most representative task and the largest open-sourced satellite image dataset, we show an obvious gain (12% for intensity forecasting) after appropriately integrating vision and physics. Through the ablation study, we quantify the benefits of (1) integrating visual data for multimodal time series forecasting (8% for intensity forecasting) and (2) integrating physics knowledge (6% for intensity forecasting).

2 Related Work

2.1 Transformers for Time-series Forecasting

Transformers are widely used for time series forecasting, demonstrating superior performance over traditional statistical models and RNN [42] architectures. Key innovations driving this success include efficient attention mechanisms and architectural adaptations tailored to temporal patterns. Recent works have introduced several enhancements to address computational complexity and domain-specific challenges. Informer [61] tackles the quadratic complexity of standard self-attention through ProbSparse attention combined with distillation operations to prioritize crucial temporal features. Autoformer [57] integrates decomposition from time-series analysis with autocorrelation-inspired attention and outperforms self-attention in both efficiency and accuracy. iTransformer [31] applies the attention and network on the inverted dimensions for time series forecasting. One Fits All [62] fine-tunes on all major types of tasks involving time series. Other variations on transformer include CrossFormer [51], TimeXer [53], TimeMixer [50], etc.

The patching paradigm has inspired multiple variants. PatchTST [34] segments time series into local windows as input tokens while maintaining channel independence for multivariate data. Building on this concept, works such as Pathformer [5] and Sageformer [59] research transformer-based patching technology in terms of multiscale and inter-series dependencies. Notably, works such as One Fits All [62] and Time-LLM [17] demonstrate the transferability of patching strategies by adapting pre-trained large language models to time-series forecasting through input token alignment.

However, these developments underscore the challenge of managing complexity when incorporating additional modules, such as patch-based components. Our method incorporates physical information via Position IDs, avoiding the need for extra models.

2.2 Multimodal LLMs for Time Series Forecasting

Recent advances in LLMs have catalyzed efforts to develop multimodal models capable of processing diverse data modalities (e.g., text, images, audio) through unified architectures. This paradigm has inspired time-series forecasting adaptations that integrate textual instructions with temporal data. TimeLLM [17] reprograms the input time series with text timestamps as prefix-prompts to align the two modalities. Unitime [29] utilizes prefix-prompts to encode frequency information of temporal data to augment the model. AutoTimes [32] uses the embedding of textual timestamps as the position encoding to incorporate temporal information. Subsequent works like UrbanGPT [25], TEST [45], ChatTime [49], and GPR4MTS [16] utilize similar methods, aligning text instructions and time series for the augmentation of time series forecasting.

However, for time series forecasting, existing multimodal approaches focus narrowly on aligning textual instructions with numerical time series, neglecting critical vision modalities inherent to many forecasting scenarios, such as typhoon forecasting. Our work researches the utilization of vision data for time series forecasting.

2.3 Position Encoding in Transformers

Transformers require explicit position encoding to capture sequential order information, unlike RNNs that inherently model temporal relationships through hidden state propagation. Current position encoding strategies can be categorized into two primary paradigms:

[1] https://github.com/hobolee/PIPE

1. Absolute position encodes the absolute position of a unit within a sentence. The original Transformer architecture [47] introduced two variants: 1) Learned positional embeddings during training stages. 2) Fixed sinusoidal functions:

$$PE_{(pos,2i)} = sin(\frac{pos}{10000^{2i/d_{model}}}) \\ PE_{(pos,2i+1)} = cos(\frac{pos}{10000^{2i/d_{model}}}) \tag{1}$$

where i denotes the dimension, pos is the position, and d_{model} is the dimension of embeddings. This matrix is simply added to the embeddings before they are fed to the Transformer model. Subsequent methods have been proposed to address the challenges of long sequences [20, 30] and improve efficiency [39].

2. Relative position encodes the position of a unit relative to other units. Shaw et al. [43] pioneered this approach by modifying self-attention to compute relative position biases. Transformer-XL [8] introduces recurrence-aware position encoding for long-context modeling. Ke et al. [19] propose untied position embeddings to add relative position embeddings through additive scalar biases. Wu et al. [54] propose to incorporate the real distances between tokens to re-scale the raw self-attention weights. Rotary Position Embedding (RoPE) [44] injects relative positions via rotation matrices.

Though effective for local sequence modeling, these methods focus on intra-instance positional relationships within individual input samples. For time-series forecasting tasks where cross-instance physical dependencies are critical (e.g., all instances share the global knowledge of geographic information), existing approaches fail to capture global temporal-spatial correlations across the entire dataset. Our work addresses this limitation through physics-informed position encoding. By encoding global timestamps with geographic coordinates (latitude/longitude), our method preserves continuous spatiotemporal relationships across independent time-series sequences.

3 Method

This section formalizes the multimodal time series forecasting problem and proposes physics-informed positional encoding that integrates physical information into VLMs for multimodal time series forecasting. A schematic overview of the method is provided in Figure 2.

3.1 Multimodal Time Series Forecasting Problem Formulation

We address the problem of multimodal time series forecasting, where historical observations comprise both time series data of multiple variables and visual images. Given a sequence of historical time steps:

$$\boldsymbol{x}_{t-H+1:t} = \{\boldsymbol{x}_{t-H+1}, \boldsymbol{x}_{t-H+2}, ..., \boldsymbol{x}_t\} \in \mathbb{R}^{H \times C} \tag{2}$$

where H denotes the historical time steps, C the number of variates, along with a corresponding sequence of H images: $\boldsymbol{i}_{t-H+1:t} \in \mathbb{R}^{3 \times H_{img} \times W_{img}}$ for each time step with H_{img}, W_{img} as the height and width of the image, the objective is to forecast the future F time steps:

$$\boldsymbol{x}_{t+1:t+F} = \{\boldsymbol{x}_{t+1}, \boldsymbol{x}_{t+2}, ..., \boldsymbol{x}_{t+F}\} \in \mathbb{R}^{F \times C} \tag{3}$$

Our task is to propose a VLM model as a cross-modal forecaster $f_{VLM}(\cdot)$ to model cross-modal relationships between the multivariate sequence $\boldsymbol{x}_{t-H+1:t}$ and visual sequence $\boldsymbol{i}_{t-H+1:t}$. Formally, we seek to learn:

$$\hat{\boldsymbol{x}}_{t+1:t+F} = f_{VLM}(\boldsymbol{x}_{t-H+1:t},\ \boldsymbol{i}_{t-H+1:t}) \tag{4}$$

3.2 VLMs for Multimodal Time Series Forecasting

To perform the multimodal time series forecasting, we use the VLM to encode the time series input and the vision input, following the practice of VLM's pipeline. In this paper, we use the open-source Qwen-2.5-vl [2] as it incorporates 3D positional encoding, which enhances its multimodal abilities.

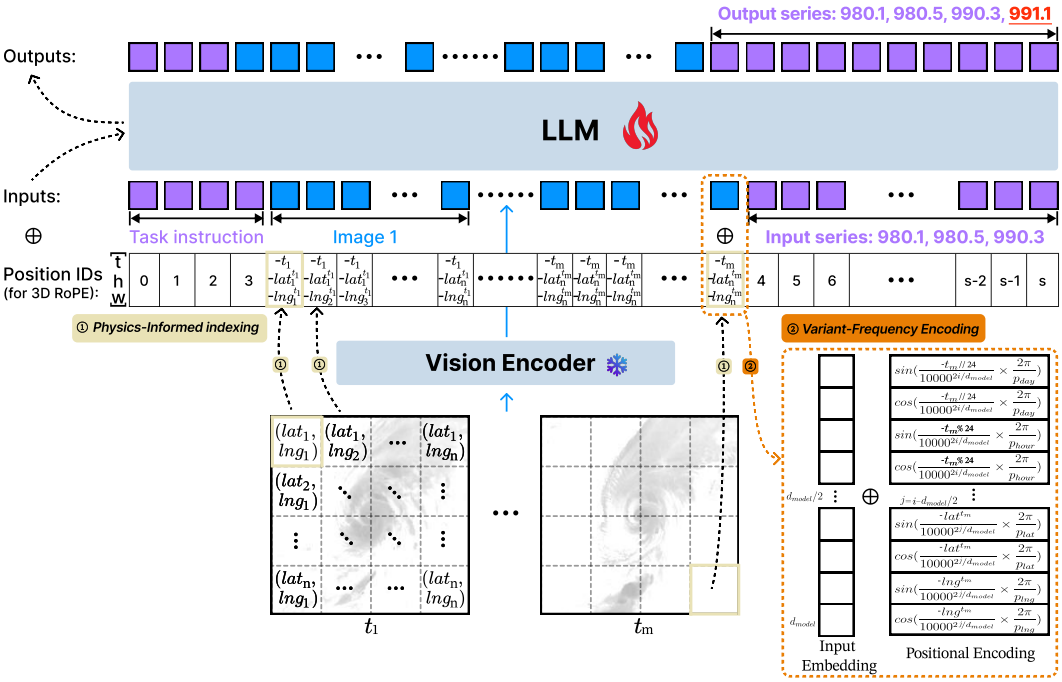

Figure 2: The framework of physics-informed positional encoding. It includes: (1) a physics-informed positional indexing scheme that maps physics to positional IDs, and (2) variant-frequency positional encoding that integrates the attributes of physical variables in the input embedding space.

Text embedding To leverage the capability of the pretrained LLM, we tokenize the time series data, $\boldsymbol{x}_{t-H+1:t}$, into tokens and concatenate them with task-specific instructions (e.g., "Predict next 24 hours of typhoon track"). They are fed into the LLM's transformer layers, as depicted with purple inputs in Figure 2. The LLM is trained during the training stage. The prompt design for multimodal time series forecasting can be found in Appendix A.

Vision embedding Each image $\boldsymbol{i}_t \in \mathbb{R}^{3\times H_{img}\times W_{img}}$ is split into N non-overlapping patches $\{\boldsymbol{p_{t,k}}\}_{k=1}^{N}$, where $\boldsymbol{p_{t,k}} \in \mathbb{R}^{3\times 28\times 28}$. These patches are encoded using the pretrained vision encoder of Qwen-2.5-vl, producing embeddings that are dimensionally consistent with the text tokens, as depicted with blue inputs in Figure 2. The vision encoder is frozen during the training stage.

3.3 PIPE

We propose **PIPE** to incorporate physical information into multimodal alignment for multimodal time series forecasting. Our proposed **PIPE** includes two cores: physics-informed positional indexing (Figure 2 ①) and variant-frequency positional encoding (Figure 2 ②). The algorithm can be found in Appendix B.

3.3.1 Physics-Informed Positional Indexing

We propose physics-informed positional indexing to integrate physical information into the model.

Schemes of indexing position IDs. Incorporating physical information into the model using positional IDs provides a direct solution without the need for additional structural complexity. We explore three indexing strategies to facilitate this integration:

(1) Sequential indexing. The most intuitive approach is to follow the standard transformer practice [47] and ViT [11], using the sequence to index the position IDs. In this scheme, the positional IDs are indexed linearly as:

$$position\_ids = [0, 1, 2, \ldots, seq\_len - 1] \tag{5}$$

where seq_len represents the total length of the input sequence, including both text tokens and vision tokens. This approach effectively encodes 1D sequential order but lacks explicit order information of the image (2D) or video (3D) for multimodal inputs.

(2) 3D indexing. Building on Qwen-2.5-VL [2], this method expands positional indexing to include three independent dimensions: temporal, height, and width, for the alignment of images and videos.

- Text tokens continue to use sequential indexing described in Equation 5, while vision tokens are indexed based on their temporal and spatial attributes.
- Temporal positions of vision tokens are calculated as:

$$t = tokens\_per\_second \times temporal\_patch\_size/fps \tag{6}$$

  where $tokens\_per\_second$ dictates how many time steps are conceptually packed into a one-second interval of the video, $temporal\_patch\_size$ is the number of frames, and fps is the video's frame rate.
- For spatial dimensions of vision tokens, the height and width positional IDs correspond to a patch grid ranging from $(0, 0)$ to $(N_{row} - 1, N_{col} - 1)$, where N_{row} and N_{col} are the numbers of image patching in height and width, respectively. Although this 3D indexing scheme aligns temporal and spatial order within vision tokens, it only captures the intra-relationship of positions with the input instance. It does not explicitly encode extra-physical properties such as time, latitude, and longitude, which are global knowledge among all instances in the dataset.

(3) Physics-Informed positional indexing (Figure 2). To address the limitations of 3D indexing, we propose a novel physics-informed positional indexing scheme that explicitly integrates global knowledge of physical attributes into positional IDs.

- Text embeddings continue to use the sequence indexing scheme described in Equation 5.
- Temporal positional IDs of vision tokens are computed based on the hourly progression of a given year. Specifically, the temporal position ID is calculated by:

$$t = t_{day} \times 24 + t_{hour} \tag{7}$$

  where t_{day} is the day of the year (ranging from 0 to 365) and t_{hour} represents the hour of the day (ranging from 0 to 23). This indexing introduces meaningful temporal patterns aligned with real-world time progression.
- The height and width positional IDs of vision tokens are determined using the latitude and longitude of the image patch centers.

To prevent the performance decreases caused by the conflicts between the physical information of vision tokens and the order information of text tokens (refer to the ablation experiment section 4.6), we map the range of vision positional IDs (t: $0 - 8784$ (8784 hours in a year), lat: $0 - 180$, lng: $0 - 360$) to negative values. This avoids overlap with the text positional ID range, ensuring smooth multimodal integration. Moreover, temporal, latitudinal, and longitudinal dimensions are inherently independent, eliminating concerns about overlap.

After incorporating the cross-instance physical information among all input samples using physics-informed positional indexing, we apply RoPE [44] on position IDs to encode intra-instance positional relationships within individual input samples.

3.3.2 Variant-Frequency Positional Encoding

We also merge the information of the physical variables into input embeddings. To differentiate between physical variables, we modify the standard sinusoidal positional encoding (Equation 1) by introducing a variant-frequency sinusoidal function.

Variant-frequency sinusoidal function This function modifies the sine and cosine components and the target dimension based on the temporal, latitude, and longitude frequencies. Figure 2 illustrates the setting, Equation 9 in the Appendix gives the complete definition, and Figure 4 visualizes

the function. For conciseness, the function for image tokens can be formulated as:

$$PE_{(pos,2i)} = sin(\frac{pos}{10000^{2i/d_{model}}} \times \frac{2\pi}{p}) \tag{8}$$
$$PE_{(pos,2i+1)} = cos(\frac{pos}{10000^{2i/d_{model}}} \times \frac{2\pi}{p})$$

where pos can be t_{day}, t_{hour}, lat, and lng depending on the dimensions. t_{day} is the day of the year (ranging from 0 to 365) and t_{hour} represents the hour of the day (ranging from 0 to 23). lat is the latitude of the image token, and lng is the longitude of the image token. p represents the wavelength specific to physics. For temporal data, $p_{day} = 366$ and $p_{hour} = 24$ and for spatial dimensions, $p_{latitude} = 180$ and $p_{longitude} = 360$. After the modification, the wavelengths form a geometric progression from p to $p \cdot 10000/2$ for vision data.

Text tokens preserve the standard sinusoidal encoding to maintain compatibility with pretrained LLM structures. These variant-frequency position encodings are added to the input embeddings at the bottom of the decoder stacks after they are divided by d_{model}. They map different physical variables to distinct frequency domains before incorporating them into the input embedding space.

4 Experiments

This section presents a systematic evaluation of the proposed method for the most representative multimodal time series forecasting task, typhoon forecasting. We first describe the datasets, baseline methods, and evaluation metrics, followed by the experiments and ablation studies.

4.1 Dataset

For multimodal time series forecasting, we utilize the open-source Digital Typhoon dataset [22], the longest hourly satellite imagery collection dedicated to typhoon analysis spanning 40+ years (1978–2023) with a 5 km spatial resolution. The spatial coverage of the dataset is the Western North Pacific basin. The dataset includes 1,116 typhoon sequences and 192,956 images (resolution of 512×512 and resized to 224x224). The size of the dataset is different from the size in the original paper since the dataset is being regularly updated.

Typhoon track annotations, including intensity, latitude, and longitude, are sourced from the Best Track dataset [23]. It is the best estimate, a globally recognized benchmark derived from retrospective post-event analysis. This metadata ensures reliable spatiotemporal grounding, as it synthesizes all available observational data to reconstruct each typhoon's lifecycle with high precision. In our experiments, we will forecast three variables: intensity, latitude, and longitude. The dataset is split using a ratio of 0.7:0.15:0.15 based on the typhoon sequences as the original dataset.

4.2 Baselines

Domain models For typhoon forecasting, we compare our method against the state-of-the-art domain-specific NWP-based model: forecasting system of the European Centre for Medium-Range Weather Forecasts (ECMWF) [10] and two environment-domain large models, Pangu [3] and GenCast [40], which serve as domain-specific benchmarks. Additionally, we include comparisons with the domain practice method, Typhoon Intensity Forecasting based on the SHIPS method (TIFS) [35]. We report only the available performance from their paper and do not retrain the models, as we cannot reproduce these domain models.

AI models We train the state-of-the-art AI models with our dataset, including Transformer-based models (PatchTST [34], iTransformer [31], Crossformer [51], TimeXer [53]) and linear-based models (TiDE [9]), LLM-based model (One Fits ALL [62], AutoTimes [32]), and other models (TimesNet [55], TimeMixer [50]). Due to their model design, they do not incorporate visual data. For the visual data integration, we include benchmark results reported in the original dataset publication (only the leading time of 12h is available) [22], closed-source Gemini-2.5-flash [6] (zero-shot), and train the original Qwen-2.5-VL [2].

Table 1: Multimodal time series forecasting results (leading time is 6h).

	Models	Intensity (hPa) MAE	Intensity (hPa) RMSE	Latitude (°) MAE	Latitude (°) RMSE	Longitude (°) MAE	Longitude (°) RMSE	Distance (km) MAE
domain	ECMWF-HRES [10]	\	\	\	\	\	\	27.181
	PanGu [3]							32.892
	GenCast [40]							20.331
	TIFS [35]	\	7.292					\
w/o vision	PatchTST [34]	1.806	<u>2.867</u>	0.199	0.266	0.322	0.404	44.537
	iTransformer [31]	1.848	2.979	0.164	0.231	0.203	0.281	31.248
	Crossformer [51]	2.389	3.599	0.310	0.418	0.520	0.684	71.216
	TimeXer [53])	3.037	4.523	0.306	0.411	0.411	0.538	59.720
	TiDE [9]	1.724	**2.819**	0.161	0.224	0.237	0.312	34.068
	One Fits All [62])	1.849	2.976	0.170	0.239	0.211	0.290	32.450
	AutoTimes [32]	1.991	3.088	0.190	0.265	0.279	0.364	40.036
	TimesNet [55]	2.401	3.711	0.465	0.630	0.855	1.124	113.718
	TimeMixer [50]	1.913	2.973	0.177	0.237	0.238	0.313	35.374
vision	Gemini-2.5-flash [6]	1.924	3.654	0.174	0.254	0.237	0.798	36.006
	Qwen-2.5-VL-3B [2]	<u>1.617</u>	3.231	<u>0.087</u>	<u>0.162</u>	<u>0.103</u>	<u>0.187</u>	<u>17.129</u>
	PIPE-3B	**1.515**	2.981	**0.084**	**0.159**	**0.095**	**0.178**	**16.275**

Implementation Details Both our method and baselines use the same temporal settings with the same length of input and output sequences (12h). For One Fits All and AutoTimes, we use their official implementations. Other models without vision, their implementations are through the publicly available Time-Series-Library [56]. For the Qwen-2.5-VL model and **PIPE**, we use LLama-Factory [60] for their implementation. More implementation specifics, including hyperparameters and training protocols, are detailed in Appendix C.

4.3 Evaluation Metrics

In NLP tasks, metrics such as ROUGE [26] and BLEU [37] are commonly employed as the metrics. In our cases, we focus on the numerical output. Specifically, for forecasting intensity, latitude, and longitude, we use Root Mean Square Error (RMSE) and Mean Absolute Error (MAE) as primary metrics. When the model accurately predicts these numerical values based on satellite images, we consider it to have effectively aligned the satellite imagery with the time series data. Additionally, we use geographiclib [18] to calculate the position error of typhoon tracks based on the latitude and longitude, following the domain practice.

4.4 Main Results

Short-term forecasting plays a crucial role in enabling timely decision-making. Therefore, the forecasting performance of multimodal time series models is presented for lead times of 6 hours (Table 1) and 12 hours (Table 5). The best results are emphasized in bold, while the second-best results are marked with <u>underline</u>.

Overall, our method achieves state-of-the-art performance across the majority of evaluation metrics, demonstrating the efficacy of the proposed **PIPE** in integrating physical information during multimodal alignment. For the 6-hour lead time (Table 1), our model outperforms baselines in most metrics. For example, it shows 12% improvement of MAE for typhoon intensity forecasting when compared to the best w/o vision models TiDE. The sole exception is the RMSE for intensity forecasting, where TiDE and PatchTST exhibit marginally superior performance. These results show the effectiveness of our approach. A critical observation is the consistent superiority of models incorporating vision data over unimodal alternatives. This finding emphasizes the importance of leveraging multimodal inputs to enhance forecasting accuracy in complex spatiotemporal tasks.

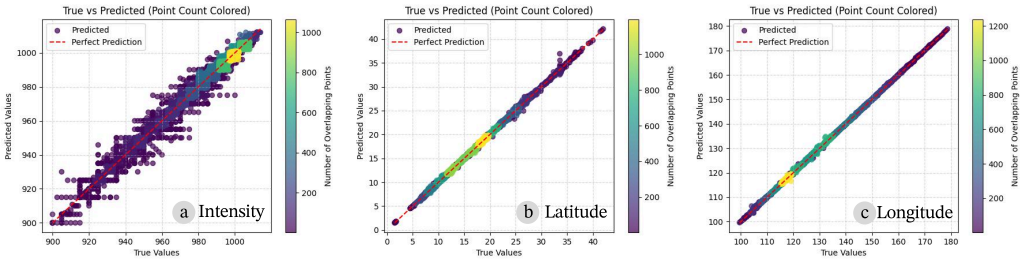

Figure 3: The visualization for the regression results between predicted values and true values (leading time is 6 hours). (a) Plots for intensity. (b) Plots for latitude. (c) Plots for longitude.

4.5 Regression Analysis

The regression results of all test typhoon sequences (Figure 3) demonstrate that our method achieves accurate typhoon predictions. Notably, the model exhibits superior performance in location forecasting compared to intensity forecasting, which may be attributed to the richer spatial information provided by satellite imagery for tracking movement. Additionally, the model shows better predictive performance when typhoon intensity is weaker (i.e., higher central pressure, around $1000\ hpa$).

4.6 Ablation Study

The results of the ablation study are presented in Table 2 and Table 6, with the best performance highlighted in **bold**. We systematically evaluate three critical components: vision inclusion, physics-informed position indexing, and variant-frequency sinusoidal function.

The gain of aligning vision The inclusion of satellite vision data yields significant improvements in forecasting accuracy. Specifically, the MAE for intensity forecasting improves by up to 8% when the leading time is set to 6 hours. This demonstrates that cross-modal learning effectively leverages spatial patterns in satellite imagery to complement time series data.

Comparison of schemes of indexing position IDs Our physics-informed indexing scheme addresses the critical challenge of preserving physical knowledge while avoiding token order conflicts. To assess its effectiveness, we compare different schemes for indexing position IDs. Specifically, we evaluate the performance by (a) removing the 3D indexing scheme (replacing it with sequential indexing), and (b) removing physics-informed indexing while retaining the 3D indexing scheme. The results show that while sequential indexing and 3D indexing perform similarly, both exhibit a noticeable performance degradation (6% for MAE of intensity forecasting) compared to the physics-informed indexing scheme. Avoiding the overlap between the physical information of vision tokens and the order information of text tokens is critical. There is a dramatic performance decrease when they share overlapping ranges (e.g., longitude: $0-360$ and text tokens: $0-seq_{len}$ (seq_{len} is the number of text tokens)). By mapping the position IDs of vision tokens to negative values, we preserve the physical information and resolve such conflicts, leading to improved performance.

The gain of integrating physical variables' frequency The incorporation of frequency characteristics of physical variables improves physical variable modeling. We show the importance by removing the entire sinusoidal function and only removing the variant-frequency sinusoidal function. The results reveal that our designed sinusoidal function plays a crucial role in aligning the model with the frequency information of physical variables. Its inclusion enhances the model's ability to leverage these variables effectively, leading to improved performance.

The necessity of combining physics-informed indexing and variant frequency positional embeddings In terms of track error, PIPE achieves an error of 16.275, compared to 16.860 when using only physics-informed indexing, 17.177 when using only variant frequency positional embeddings, and 17.129 for the baseline. These results clearly demonstrate that the combination of both components delivers the most significant performance improvement.

Table 2: The results of the ablation study (leading time is 6h).

Models	Intensity (hPa)		Latitude (°)		Longitude (°)		Distance (km)
	MAE	RMSE	MAE	RMSE	MAE	RMSE	MAE
w/o vision	1.646	3.220	0.088	0.160	0.102	0.193	17.235
w/o 3D indexing (using sequence)	1.628	3.749	0.087	0.163	0.102	0.185	17.084
w/o physics-informed indexing (using 3D)	1.617	3.231	0.087	0.162	0.103	0.187	17.129
w/o negative indexing	1.961	3.926	0.206	0.360	0.388	0.674	53.548
w/o entire sinusoidal function	1.545	3.053	0.085	**0.157**	0.097	0.180	16.554
w/o variant-frequency sinusoidal function	1.639	3.178	0.086	0.161	0.101	0.183	16.860
w/o entire physics-informed indexing	1.581	2.994	0.087	0.161	0.102	0.186	17.117
PIPE-3B	**1.515**	**2.981**	**0.084**	0.159	**0.095**	**0.178**	**16.275**

Every component contributes to the multimodal time series forecasting, with vision alignment providing complementary visual patterns, the physics-informed indexing scheme ensuring physical knowledge integration, and the variant-frequency sinusoidal function incorporating physical variables' frequency information.

4.7 Generalizability Experiment

To demonstrate the generalizability of our method, we add an additional experiment in the Australian region (AU) [21]. The settings remain the same as the main experiment. The results are shown in Table 3. The results demonstrate that our method can be applied to various regions for typhoon forecasting. Even the model trained on the West Pacific region can perform well in the new dataset (zero-shot). For instance, compared to Qwen-2.5-VL-3B (after tuning), PIPE-3B (Zero-shot) achieved a lower intensity RMSE (2.773 vs. 2.806) and a smaller distance error (19.090 vs. 19.718). Additionally, PIPE-3B (after tuning) outperformed both models, achieving the best performance.

Table 3: The results of the AU Typhoon Experiment (leading time is 6h).

Models	Intensity (hPa)		Latitude (°)		Longitude (°)		Distance (km)
	MAE	RMSE	MAE	RMSE	MAE	RMSE	MAE
Qwen-2.5-VL-3B (after tuning)	1.399	2.806	0.098	0.201	0.121	0.211	19.718
PIPE-3B (Zero-shot)	1.361	2.773	0.094	0.171	0.118	0.206	19.090
PIPE-3B (after tuning)	**1.352**	**2.558**	**0.093**	**0.163**	**0.116**	**0.202**	**18.835**

5 Limitation

While the integration of satellite imagery improves forecasting accuracy, it increases the computational complexity needed to process high-resolution images. To address these limitations, future work will focus on improving the efficiency of integrating vision data into forecasting models to enable longer input sequences and extended forecasting horizons for VLMs. Furthermore, we will explore the incorporation of physical laws or constraints. Beyond embedding physical information, integrating domain-specific physical principles or environmental constraints could improve the model's interpretability and robustness.

6 Conclusion

This paper proposes a multimodal time series forecasting task and addresses the challenge brought by integrating satellite imagery. Existing approaches only focus on pixel-level features, overlooking the rich temporal and geophysical context embedded within vision data. We propose **p**hysics-**i**nformed **p**osition **e**ncoding (**PIPE**). Experimental results demonstrate that **PIPE** achieves state-of-the-art performance across multiple benchmarks. Ablation studies further validate the distinct contributions of each component. Future work will explore the integration of additional physical domain knowledge, such as physical laws and constraints, to enhance real-world applicability.

Acknowledgements

This project is partially supported by RGC TRS grant T22-607/24N and a grant from the Research Grants Council of the Hong Kong Special Administrative Region, China (Project No. RMGS20RG01).

References

[1] Samira Abnar and Willem Zuidema. Quantifying attention flow in transformers. In Dan Jurafsky, Joyce Chai, Natalie Schluter, and Joel Tetreault, editors, *Proceedings of the 58th Annual Meeting of the Association for Computational Linguistics*, pages 4190–4197, Online, July 2020. Association for Computational Linguistics.

[2] Shuai Bai, Keqin Chen, Xuejing Liu, Jialin Wang, Wenbin Ge, Sibo Song, Kai Dang, Peng Wang, Shijie Wang, Jun Tang, Humen Zhong, Yuanzhi Zhu, Mingkun Yang, Zhaohai Li, Jianqiang Wan, Pengfei Wang, Wei Ding, Zheren Fu, Yiheng Xu, Jiabo Ye, Xi Zhang, Tianbao Xie, Zesen Cheng, Hang Zhang, Zhibo Yang, Haiyang Xu, and Junyang Lin. Qwen2.5-vl technical report. *arXiv preprint arXiv:2502.13923*, 2025.

[3] Kaifeng Bi, Lingxi Xie, Hengheng Zhang, Xin Chen, Xiaotao Gu, and Qi Tian. Accurate medium-range global weather forecasting with 3d neural networks. *Nature*, 619(7970):533–538, 2023.

[4] Ching Chang, Wei-Yao Wang, Wen-Chih Peng, and Tien-Fu Chen. Llm4ts: Aligning pre-trained llms as data-efficient time-series forecasters. *ACM Trans. Intell. Syst. Technol.*, 16(3), April 2025.

[5] Peng Chen, Yingying Zhang, Yunyao Cheng, Yang Shu, Yihang Wang, Qingsong Wen, Bin Yang, and Chenjuan Guo. Pathformer: Multi-scale transformers with adaptive pathways for time series forecasting. *arXiv preprint arXiv:2402.05956*, 2024.

[6] Gheorghe Comanici, Eric Bieber, Mike Schaekermann, Ice Pasupat, Noveen Sachdeva, Inderjit Dhillon, Marcel Blistein, Ori Ram, Dan Zhang, Evan Rosen, et al. Gemini 2.5: Pushing the frontier with advanced reasoning, multimodality, long context, and next generation agentic capabilities. *arXiv preprint arXiv:2507.06261*, 2025.

[7] John Dagdelen, Alexander Dunn, Sanghoon Lee, Nicholas Walker, Andrew S Rosen, Gerbrand Ceder, Kristin A Persson, and Anubhav Jain. Structured information extraction from scientific text with large language models. *Nature Communications*, 15(1):1418, 2024.

[8] Zihang Dai, Zhilin Yang, Yiming Yang, Jaime Carbonell, Quoc Le, and Ruslan Salakhutdinov. Transformer-XL: Attentive language models beyond a fixed-length context. In Anna Korhonen, David Traum, and Lluís Màrquez, editors, *Proceedings of the 57th Annual Meeting of the Association for Computational Linguistics*, pages 2978–2988, Florence, Italy, July 2019. Association for Computational Linguistics.

[9] Abhimanyu Das, Weihao Kong, Andrew Leach, Shaan Mathur, Rajat Sen, and Rose Yu. Long-term forecasting with tide: Time-series dense encoder. *arXiv preprint arXiv:2304.08424*, 2023.

[10] IFS DOCUMENTATION-Cy40r1. Part v: Ensemble prediction system. 2020.

[11] Alexey Dosovitskiy, Lucas Beyer, Alexander Kolesnikov, Dirk Weissenborn, Xiaohua Zhai, Thomas Unterthiner, Mostafa Dehghani, Matthias Minderer, Georg Heigold, Sylvain Gelly, et al. An image is worth 16x16 words: Transformers for image recognition at scale. *arXiv preprint arXiv:2010.11929*, 2020.

[12] Siu Lau Ho and Min Xie. The use of arima models for reliability forecasting and analysis. *Computers & industrial engineering*, 35(1-2):213–216, 1998.

[13] Sepp Hochreiter and Jürgen Schmidhuber. Long short-term memory. *Neural computation*, 9(8):1735–1780, 1997.

[14] Edward J Hu, Yelong Shen, Phillip Wallis, Zeyuan Allen-Zhu, Yuanzhi Li, Shean Wang, Lu Wang, Weizhu Chen, et al. Lora: Low-rank adaptation of large language models. *ICLR*, 1(2):3, 2022.

[15] Neal Jean, Marshall Burke, Michael Xie, W Matthew Alampay Davis, David B Lobell, and Stefano Ermon. Combining satellite imagery and machine learning to predict poverty. *Science*, 353(6301):790–794, 2016.

[16] Furong Jia, Kevin Wang, Yixiang Zheng, Defu Cao, and Yan Liu. Gpt4mts: Prompt-based large language model for multimodal time-series forecasting. In *Proceedings of the AAAI Conference on Artificial Intelligence*, volume 38, pages 23343–23351, 2024.

[17] Ming Jin, Shiyu Wang, Lintao Ma, Zhixuan Chu, James Y Zhang, Xiaoming Shi, Pin-Yu Chen, Yuxuan Liang, Yuan-Fang Li, Shirui Pan, and Qingsong Wen. Time-LLM: Time series forecasting by reprogramming large language models. In *International Conference on Learning Representations (ICLR)*, 2024.

[18] Charles FF Karney. Algorithms for geodesics. *Journal of Geodesy*, 87:43–55, 2013.

[19] Guolin Ke, Di He, and Tie-Yan Liu. Rethinking positional encoding in language pre-training. In *International Conference on Learning Representations*, 2021.

[20] Nikita Kitaev, Lukasz Kaiser, and Anselm Levskaya. Reformer: The efficient transformer. In *International Conference on Learning Representations*, 2020.

[21] Asanobu Kitamoto, Erwan Dzik, and Gaspar Faure. Machine learning for the digital typhoon dataset: Extensions to multiple basins and new developments in representations and tasks. *arXiv preprint arXiv:2411.16421*, 2024.

[22] Asanobu Kitamoto, Jared Hwang, Bastien Vuillod, Lucas Gautier, Yingtao Tian, and Tarin Clanuwat. Digital typhoon: Long-term satellite image dataset for the spatio-temporal modeling of tropical cyclones. *Advances in Neural Information Processing Systems*, 36:40623–40636, 2023.

[23] Kenneth R Knapp, Michael C Kruk, David H Levinson, Howard J Diamond, and Charles J Neumann. The international best track archive for climate stewardship (ibtracs) unifying tropical cyclone data. *Bulletin of the American Meteorological Society*, 91(3):363–376, 2010.

[24] Junnan Li, Dongxu Li, Silvio Savarese, and Steven Hoi. Blip-2: Bootstrapping language-image pre-training with frozen image encoders and large language models. In *International conference on machine learning*, pages 19730–19742. PMLR, 2023.

[25] Zhonghang Li, Lianghao Xia, Jiabin Tang, Yong Xu, Lei Shi, Long Xia, Dawei Yin, and Chao Huang. Urbangpt: Spatio-temporal large language models. In *Proceedings of the 30th ACM SIGKDD Conference on Knowledge Discovery and Data Mining*, pages 5351–5362, 2024.

[26] Chin-Yew Lin. ROUGE: A package for automatic evaluation of summaries. In *Text Summarization Branches Out*, pages 74–81, Barcelona, Spain, July 2004. Association for Computational Linguistics.

[27] Hezheng Lin, Xing Cheng, Xiangyu Wu, and Dong Shen. Cat: Cross attention in vision transformer. In *2022 IEEE international conference on multimedia and expo (ICME)*, pages 1–6. IEEE, 2022.

[28] Haotian Liu, Chunyuan Li, Qingyang Wu, and Yong Jae Lee. Visual instruction tuning. *Advances in neural information processing systems*, 36:34892–34916, 2023.

[29] Xu Liu, Junfeng Hu, Yuan Li, Shizhe Diao, Yuxuan Liang, Bryan Hooi, and Roger Zimmermann. Unitime: A language-empowered unified model for cross-domain time series forecasting. In *Proceedings of the ACM Web Conference 2024*, pages 4095–4106, 2024.

[30] Xuanqing Liu, Hsiang-Fu Yu, Inderjit Dhillon, and Cho-Jui Hsieh. Learning to encode position for transformer with continuous dynamical model. In Hal Daumé III and Aarti Singh, editors, *Proceedings of the 37th International Conference on Machine Learning*, volume 119 of *Proceedings of Machine Learning Research*, pages 6327–6335. PMLR, 13–18 Jul 2020.

[31] Yong Liu, Tengge Hu, Haoran Zhang, Haixu Wu, Shiyu Wang, Lintao Ma, and Mingsheng Long. itransformer: Inverted transformers are effective for time series forecasting. *arXiv preprint arXiv:2310.06625*, 2023.

[32] Yong Liu, Guo Qin, Xiangdong Huang, Jianmin Wang, and Mingsheng Long. Autotimes: Autoregressive time series forecasters via large language models. *arXiv preprint arXiv:2402.02370*, 2024.

[33] Ilya Loshchilov and Frank Hutter. Decoupled weight decay regularization. *arXiv preprint arXiv:1711.05101*, 2017.

[34] Yuqi Nie, Nam H Nguyen, Phanwadee Sinthong, and Jayant Kalagnanam. A time series is worth 64 words: Long-term forecasting with transformers. *arXiv preprint arXiv:2211.14730*, 2022.

[35] Marika Ono, Shoji Notsuhara, Junya Fukuda, Yohko Igarashi, and Kotaro Bessho. Operational use of the typhoon intensity forecasting scheme based on ships (tifs) and commencement of five-day tropical cyclone intensity forecasts. *ENE*, 128(40):128–7, 2019.

[36] OpenAI et al. Gpt-4 technical report, 2024.

[37] Kishore Papineni, Salim Roukos, Todd Ward, and Wei-Jing Zhu. Bleu: a method for automatic evaluation of machine translation. In *Proceedings of the 40th annual meeting of the Association for Computational Linguistics*, pages 311–318, 2002.

[38] Adam Paszke, Sam Gross, Francisco Massa, Adam Lerer, James Bradbury, Gregory Chanan, Trevor Killeen, Zeming Lin, Natalia Gimelshein, Luca Antiga, Alban Desmaison, Andreas Kopf, Edward Yang, Zachary DeVito, Martin Raison, Alykhan Tejani, Sasank Chilamkurthy, Benoit Steiner, Lu Fang, Junjie Bai, and Soumith Chintala. Pytorch: An imperative style, high-performance deep learning library. In H. Wallach, H. Larochelle, A. Beygelzimer, F. d'Alché-Buc, E. Fox, and R. Garnett, editors, *Advances in Neural Information Processing Systems*, volume 32. Curran Associates, Inc., 2019.

[39] Ofir Press, Noah A. Smith, and Mike Lewis. Shortformer: Better language modeling using shorter inputs. In Chengqing Zong, Fei Xia, Wenjie Li, and Roberto Navigli, editors, *Proceedings of the 59th Annual Meeting of the Association for Computational Linguistics and the 11th International Joint Conference on Natural Language Processing (Volume 1: Long Papers)*, pages 5493–5505, Online, August 2021. Association for Computational Linguistics.

[40] Ilan Price, Alvaro Sanchez-Gonzalez, Ferran Alet, Tom R Andersson, Andrew El-Kadi, Dominic Masters, Timo Ewalds, Jacklynn Stott, Shakir Mohamed, Peter Battaglia, et al. Probabilistic weather forecasting with machine learning. *Nature*, 637(8044):84–90, 2025.

[41] Alec Radford, Jong Wook Kim, Chris Hallacy, Aditya Ramesh, Gabriel Goh, Sandhini Agarwal, Girish Sastry, Amanda Askell, Pamela Mishkin, Jack Clark, et al. Learning transferable visual models from natural language supervision. In *International conference on machine learning*, pages 8748–8763. PmLR, 2021.

[42] David E Rumelhart, Geoffrey E Hinton, and Ronald J Williams. Learning representations by back-propagating errors. *nature*, 323(6088):533–536, 1986.

[43] Peter Shaw, Jakob Uszkoreit, and Ashish Vaswani. Self-attention with relative position representations. In Marilyn Walker, Heng Ji, and Amanda Stent, editors, *Proceedings of the 2018 Conference of the North American Chapter of the Association for Computational Linguistics: Human Language Technologies, Volume 2 (Short Papers)*, pages 464–468, New Orleans, Louisiana, June 2018. Association for Computational Linguistics.

[44] Jianlin Su, Murtadha Ahmed, Yu Lu, Shengfeng Pan, Wen Bo, and Yunfeng Liu. Roformer: Enhanced transformer with rotary position embedding. *Neurocomput.*, 568(C), February 2024.

[45] Chenxi Sun, Hongyan Li, Yaliang Li, and Shenda Hong. TEST: Text prototype aligned embedding to activate LLM's ability for time series. In *The Twelfth International Conference on Learning Representations*, 2024.

[46] Gemini Team, Rohan Anil, Sebastian Borgeaud, Yonghui Wu, Jean-Baptiste Alayrac, Jiahui Yu, Radu Soricut, Johan Schalkwyk, Andrew M Dai, Anja Hauth, et al. Gemini: a family of highly capable multimodal models. *arXiv preprint arXiv:2312.11805*, 2023.

[47] Ashish Vaswani, Noam Shazeer, Niki Parmar, Jakob Uszkoreit, Llion Jones, Aidan N Gomez, Łukasz Kaiser, and Illia Polosukhin. Attention is all you need. *Advances in neural information processing systems*, 30, 2017.

[48] Mark Veillette, Siddharth Samsi, and Chris Mattioli. Sevir: A storm event imagery dataset for deep learning applications in radar and satellite meteorology. *Advances in Neural Information Processing Systems*, 33:22009–22019, 2020.

[49] Chengsen Wang, Qi Qi, Jingyu Wang, Haifeng Sun, Zirui Zhuang, Jinming Wu, Lei Zhang, and Jianxin Liao. Chattime: A unified multimodal time series foundation model bridging numerical and textual data. In *Proceedings of the AAAI Conference on Artificial Intelligence*, volume 39, pages 12694–12702, 2025.

[50] Shiyu Wang, Haixu Wu, Xiaoming Shi, Tengge Hu, Huakun Luo, Lintao Ma, James Y Zhang, and Jun Zhou. Timemixer: Decomposable multiscale mixing for time series forecasting. *arXiv preprint arXiv:2405.14616*, 2024.

[51] Wenxiao Wang, Wei Chen, Qibo Qiu, Long Chen, Boxi Wu, Binbin Lin, Xiaofei He, and Wei Liu. Crossformer++: A versatile vision transformer hinging on cross-scale attention. *IEEE Transactions on Pattern Analysis and Machine Intelligence*, 46(5):3123–3136, 2023.

[52] Yihe Wang, Yu Han, Haishuai Wang, and Xiang Zhang. Contrast everything: A hierarchical contrastive framework for medical time-series. *Advances in Neural Information Processing Systems*, 36:55694–55717, 2023.

[53] Yuxuan Wang, Haixu Wu, Jiaxiang Dong, Guo Qin, Haoran Zhang, Yong Liu, Yunzhong Qiu, Jianmin Wang, and Mingsheng Long. Timexer: Empowering transformers for time series forecasting with exogenous variables. *arXiv preprint arXiv:2402.19072*, 2024.

[54] Chuhan Wu, Fangzhao Wu, and Yongfeng Huang. DA-transformer: Distance-aware transformer. In Kristina Toutanova, Anna Rumshisky, Luke Zettlemoyer, Dilek Hakkani-Tur, Iz Beltagy, Steven Bethard, Ryan Cotterell, Tanmoy Chakraborty, and Yichao Zhou, editors, *Proceedings of the 2021 Conference of the North American Chapter of the Association for Computational Linguistics: Human Language Technologies*, pages 2059–2068, Online, June 2021. Association for Computational Linguistics.

[55] Haixu Wu, Tengge Hu, Yong Liu, Hang Zhou, Jianmin Wang, and Mingsheng Long. Timesnet: Temporal 2d-variation modeling for general time series analysis. *arXiv preprint arXiv:2210.02186*, 2022.

[56] Haixu Wu, Tengge Hu, Yong Liu, Hang Zhou, Jianmin Wang, and Mingsheng Long. Timesnet: Temporal 2d-variation modeling for general time series analysis. In *International Conference on Learning Representations*, 2023.

[57] Haixu Wu, Jiehui Xu, Jianmin Wang, and Mingsheng Long. Autoformer: Decomposition transformers with auto-correlation for long-term series forecasting. *Advances in neural information processing systems*, 34:22419–22430, 2021.

[58] Yuan Yuan and Lei Lin. Self-supervised pretraining of transformers for satellite image time series classification. *IEEE Journal of Selected Topics in Applied Earth Observations and Remote Sensing*, 14:474–487, 2020.

[59] Zhenwei Zhang, Linghang Meng, and Yuantao Gu. Sageformer: Series-aware framework for long-term multivariate time-series forecasting. *IEEE Internet of Things Journal*, 11(10):18435–18448, 2024.

[60] Yaowei Zheng, Richong Zhang, Junhao Zhang, Yanhan Ye, Zheyan Luo, Zhangchi Feng, and Yongqiang Ma. Llamafactory: Unified efficient fine-tuning of 100+ language models. In *Proceedings of the 62nd Annual Meeting of the Association for Computational Linguistics (Volume 3: System Demonstrations)*, Bangkok, Thailand, 2024. Association for Computational Linguistics.

[61] Haoyi Zhou, Shanghang Zhang, Jieqi Peng, Shuai Zhang, Jianxin Li, Hui Xiong, and Wancai Zhang. Informer: Beyond efficient transformer for long sequence time-series forecasting. In *Proceedings of the AAAI conference on artificial intelligence*, volume 35, pages 11106–11115, 2021.

[62] Tian Zhou, Peisong Niu, Liang Sun, Rong Jin, et al. One fits all: Power general time series analysis by pretrained lm. *Advances in neural information processing systems*, 36:43322–43355, 2023.

NeurIPS Paper Checklist

1. **Claims**

   Question: Do the main claims made in the abstract and introduction accurately reflect the paper's contributions and scope?

   Answer: [Yes]

   Justification: We state our claim and contributions in our abstract and introduction.

   Guidelines:

   - The answer NA means that the abstract and introduction do not include the claims made in the paper.
   - The abstract and/or introduction should clearly state the claims made, including the contributions made in the paper and important assumptions and limitations. A No or NA answer to this question will not be perceived well by the reviewers.
   - The claims made should match theoretical and experimental results, and reflect how much the results can be expected to generalize to other settings.
   - It is fine to include aspirational goals as motivation as long as it is clear that these goals are not attained by the paper.

2. **Limitations**

   Question: Does the paper discuss the limitations of the work performed by the authors?

   Answer: [Yes]

   Justification: We discuss the limitation in section 5.

   Guidelines:

   - The answer NA means that the paper has no limitation while the answer No means that the paper has limitations, but those are not discussed in the paper.
   - The authors are encouraged to create a separate "Limitations" section in their paper.
   - The paper should point out any strong assumptions and how robust the results are to violations of these assumptions (e.g., independence assumptions, noiseless settings, model well-specification, asymptotic approximations only holding locally). The authors should reflect on how these assumptions might be violated in practice and what the implications would be.
   - The authors should reflect on the scope of the claims made, e.g., if the approach was only tested on a few datasets or with a few runs. In general, empirical results often depend on implicit assumptions, which should be articulated.
   - The authors should reflect on the factors that influence the performance of the approach. For example, a facial recognition algorithm may perform poorly when image resolution is low or images are taken in low lighting. Or a speech-to-text system might not be used reliably to provide closed captions for online lectures because it fails to handle technical jargon.
   - The authors should discuss the computational efficiency of the proposed algorithms and how they scale with dataset size.
   - If applicable, the authors should discuss possible limitations of their approach to address problems of privacy and fairness.
   - While the authors might fear that complete honesty about limitations might be used by reviewers as grounds for rejection, a worse outcome might be that reviewers discover limitations that aren't acknowledged in the paper. The authors should use their best judgment and recognize that individual actions in favor of transparency play an important role in developing norms that preserve the integrity of the community. Reviewers will be specifically instructed to not penalize honesty concerning limitations.

3. **Theory assumptions and proofs**

   Question: For each theoretical result, does the paper provide the full set of assumptions and a complete (and correct) proof?

   Answer: [NA]

Justification: We do not include theoretical results.

Guidelines:

- The answer NA means that the paper does not include theoretical results.
- All the theorems, formulas, and proofs in the paper should be numbered and cross-referenced.
- All assumptions should be clearly stated or referenced in the statement of any theorems.
- The proofs can either appear in the main paper or the supplemental material, but if they appear in the supplemental material, the authors are encouraged to provide a short proof sketch to provide intuition.
- Inversely, any informal proof provided in the core of the paper should be complemented by formal proofs provided in appendix or supplemental material.
- Theorems and Lemmas that the proof relies upon should be properly referenced.

4. **Experimental result reproducibility**

   Question: Does the paper fully disclose all the information needed to reproduce the main experimental results of the paper to the extent that it affects the main claims and/or conclusions of the paper (regardless of whether the code and data are provided or not)?

   Answer: [Yes]

   Justification: We disclose the implementation details in section 4 and Appendix C for reproducing the results. We also provide the code and data in supplementary materials for reproduction.

   Guidelines:

   - The answer NA means that the paper does not include experiments.
   - If the paper includes experiments, a No answer to this question will not be perceived well by the reviewers: Making the paper reproducible is important, regardless of whether the code and data are provided or not.
   - If the contribution is a dataset and/or model, the authors should describe the steps taken to make their results reproducible or verifiable.
   - Depending on the contribution, reproducibility can be accomplished in various ways. For example, if the contribution is a novel architecture, describing the architecture fully might suffice, or if the contribution is a specific model and empirical evaluation, it may be necessary to either make it possible for others to replicate the model with the same dataset, or provide access to the model. In general. releasing code and data is often one good way to accomplish this, but reproducibility can also be provided via detailed instructions for how to replicate the results, access to a hosted model (e.g., in the case of a large language model), releasing of a model checkpoint, or other means that are appropriate to the research performed.
   - While NeurIPS does not require releasing code, the conference does require all submissions to provide some reasonable avenue for reproducibility, which may depend on the nature of the contribution. For example
     (a) If the contribution is primarily a new algorithm, the paper should make it clear how to reproduce that algorithm.
     (b) If the contribution is primarily a new model architecture, the paper should describe the architecture clearly and fully.
     (c) If the contribution is a new model (e.g., a large language model), then there should either be a way to access this model for reproducing the results or a way to reproduce the model (e.g., with an open-source dataset or instructions for how to construct the dataset).
     (d) We recognize that reproducibility may be tricky in some cases, in which case authors are welcome to describe the particular way they provide for reproducibility. In the case of closed-source models, it may be that access to the model is limited in some way (e.g., to registered users), but it should be possible for other researchers to have some path to reproducing or verifying the results.

5. **Open access to data and code**

Question: Does the paper provide open access to the data and code, with sufficient instructions to faithfully reproduce the main experimental results, as described in supplemental material?

Answer: [Yes]

Justification: We provide the code and data in the supplementary materials.

Guidelines:

- The answer NA means that paper does not include experiments requiring code.
- Please see the NeurIPS code and data submission guidelines (`https://nips.cc/public/guides/CodeSubmissionPolicy`) for more details.
- While we encourage the release of code and data, we understand that this might not be possible, so "No" is an acceptable answer. Papers cannot be rejected simply for not including code, unless this is central to the contribution (e.g., for a new open-source benchmark).
- The instructions should contain the exact command and environment needed to run to reproduce the results. See the NeurIPS code and data submission guidelines (`https://nips.cc/public/guides/CodeSubmissionPolicy`) for more details.
- The authors should provide instructions on data access and preparation, including how to access the raw data, preprocessed data, intermediate data, and generated data, etc.
- The authors should provide scripts to reproduce all experimental results for the new proposed method and baselines. If only a subset of experiments are reproducible, they should state which ones are omitted from the script and why.
- At submission time, to preserve anonymity, the authors should release anonymized versions (if applicable).
- Providing as much information as possible in supplemental material (appended to the paper) is recommended, but including URLs to data and code is permitted.

6. **Experimental setting/details**

   Question: Does the paper specify all the training and test details (e.g., data splits, hyperparameters, how they were chosen, type of optimizer, etc.) necessary to understand the results?

   Answer: [Yes]

   Justification: Please refer to section 4 and Appendix C for the training and test details. We introduce settings, training hyperparameters, optimizer, etc.

   Guidelines:

   - The answer NA means that the paper does not include experiments.
   - The experimental setting should be presented in the core of the paper to a level of detail that is necessary to appreciate the results and make sense of them.
   - The full details can be provided either with the code, in appendix, or as supplemental material.

7. **Experiment statistical significance**

   Question: Does the paper report error bars suitably and correctly defined or other appropriate information about the statistical significance of the experiments?

   Answer: [Yes]

   Justification: We report standard deviations with three random seeds in subsection E.2.

   Guidelines:

   - The answer NA means that the paper does not include experiments.
   - The authors should answer "Yes" if the results are accompanied by error bars, confidence intervals, or statistical significance tests, at least for the experiments that support the main claims of the paper.
   - The factors of variability that the error bars are capturing should be clearly stated (for example, train/test split, initialization, random drawing of some parameter, or overall run with given experimental conditions).

- The method for calculating the error bars should be explained (closed form formula, call to a library function, bootstrap, etc.)
- The assumptions made should be given (e.g., Normally distributed errors).
- It should be clear whether the error bar is the standard deviation or the standard error of the mean.
- It is OK to report 1-sigma error bars, but one should state it. The authors should preferably report a 2-sigma error bar than state that they have a 96% CI, if the hypothesis of Normality of errors is not verified.
- For asymmetric distributions, the authors should be careful not to show in tables or figures symmetric error bars that would yield results that are out of range (e.g. negative error rates).
- If error bars are reported in tables or plots, The authors should explain in the text how they were calculated and reference the corresponding figures or tables in the text.

8. **Experiments compute resources**

   Question: For each experiment, does the paper provide sufficient information on the computer resources (type of compute workers, memory, time of execution) needed to reproduce the experiments?

   Answer: [Yes]

   Justification: We provide the computation cost in Appendix C.

   Guidelines:

   - The answer NA means that the paper does not include experiments.
   - The paper should indicate the type of compute workers CPU or GPU, internal cluster, or cloud provider, including relevant memory and storage.
   - The paper should provide the amount of compute required for each of the individual experimental runs as well as estimate the total compute.
   - The paper should disclose whether the full research project required more compute than the experiments reported in the paper (e.g., preliminary or failed experiments that didn't make it into the paper).

9. **Code of ethics**

   Question: Does the research conducted in the paper conform, in every respect, with the NeurIPS Code of Ethics `https://neurips.cc/public/EthicsGuidelines`?

   Answer: [Yes]

   Justification: We have checked the NeurIPS Code of Ethics and our research conforms with it.

   Guidelines:

   - The answer NA means that the authors have not reviewed the NeurIPS Code of Ethics.
   - If the authors answer No, they should explain the special circumstances that require a deviation from the Code of Ethics.
   - The authors should make sure to preserve anonymity (e.g., if there is a special consideration due to laws or regulations in their jurisdiction).

10. **Broader impacts**

    Question: Does the paper discuss both potential positive societal impacts and negative societal impacts of the work performed?

    Answer: [Yes]

    Justification: We discuss the broader impacts of our work in Appendix F, including the impacts on other domains and scenarios.

    Guidelines:

    - The answer NA means that there is no societal impact of the work performed.
    - If the authors answer NA or No, they should explain why their work has no societal impact or why the paper does not address societal impact.

- Examples of negative societal impacts include potential malicious or unintended uses (e.g., disinformation, generating fake profiles, surveillance), fairness considerations (e.g., deployment of technologies that could make decisions that unfairly impact specific groups), privacy considerations, and security considerations.
- The conference expects that many papers will be foundational research and not tied to particular applications, let alone deployments. However, if there is a direct path to any negative applications, the authors should point it out. For example, it is legitimate to point out that an improvement in the quality of generative models could be used to generate deepfakes for disinformation. On the other hand, it is not needed to point out that a generic algorithm for optimizing neural networks could enable people to train models that generate Deepfakes faster.
- The authors should consider possible harms that could arise when the technology is being used as intended and functioning correctly, harms that could arise when the technology is being used as intended but gives incorrect results, and harms following from (intentional or unintentional) misuse of the technology.
- If there are negative societal impacts, the authors could also discuss possible mitigation strategies (e.g., gated release of models, providing defenses in addition to attacks, mechanisms for monitoring misuse, mechanisms to monitor how a system learns from feedback over time, improving the efficiency and accessibility of ML).

11. **Safeguards**

    Question: Does the paper describe safeguards that have been put in place for responsible release of data or models that have a high risk for misuse (e.g., pretrained language models, image generators, or scraped datasets)?

    Answer: [NA]

    Justification: Our paper poses no such risks.

    Guidelines:

    - The answer NA means that the paper poses no such risks.
    - Released models that have a high risk for misuse or dual-use should be released with necessary safeguards to allow for controlled use of the model, for example by requiring that users adhere to usage guidelines or restrictions to access the model or implementing safety filters.
    - Datasets that have been scraped from the Internet could pose safety risks. The authors should describe how they avoided releasing unsafe images.
    - We recognize that providing effective safeguards is challenging, and many papers do not require this, but we encourage authors to take this into account and make a best faith effort.

12. **Licenses for existing assets**

    Question: Are the creators or original owners of assets (e.g., code, data, models), used in the paper, properly credited and are the license and terms of use explicitly mentioned and properly respected?

    Answer: [Yes]

    Justification: We properly cite the assets including dataset and code in section 4 and Appendix C.

    Guidelines:

    - The answer NA means that the paper does not use existing assets.
    - The authors should cite the original paper that produced the code package or dataset.
    - The authors should state which version of the asset is used and, if possible, include a URL.
    - The name of the license (e.g., CC-BY 4.0) should be included for each asset.
    - For scraped data from a particular source (e.g., website), the copyright and terms of service of that source should be provided.

- If assets are released, the license, copyright information, and terms of use in the package should be provided. For popular datasets, `paperswithcode.com/datasets` has curated licenses for some datasets. Their licensing guide can help determine the license of a dataset.
- For existing datasets that are re-packaged, both the original license and the license of the derived asset (if it has changed) should be provided.
- If this information is not available online, the authors are encouraged to reach out to the asset's creators.

13. **New assets**

    Question: Are new assets introduced in the paper well documented and is the documentation provided alongside the assets?

    Answer: [Yes]

    Justification: We provide the readme file for our code in the supplementary materials.

    Guidelines:

    - The answer NA means that the paper does not release new assets.
    - Researchers should communicate the details of the dataset/code/model as part of their submissions via structured templates. This includes details about training, license, limitations, etc.
    - The paper should discuss whether and how consent was obtained from people whose asset is used.
    - At submission time, remember to anonymize your assets (if applicable). You can either create an anonymized URL or include an anonymized zip file.

14. **Crowdsourcing and research with human subjects**

    Question: For crowdsourcing experiments and research with human subjects, does the paper include the full text of instructions given to participants and screenshots, if applicable, as well as details about compensation (if any)?

    Answer: [NA]

    Justification: Our work does not involve crowdsourcing nor research with human subjects.

    Guidelines:

    - The answer NA means that the paper does not involve crowdsourcing nor research with human subjects.
    - Including this information in the supplemental material is fine, but if the main contribution of the paper involves human subjects, then as much detail as possible should be included in the main paper.
    - According to the NeurIPS Code of Ethics, workers involved in data collection, curation, or other labor should be paid at least the minimum wage in the country of the data collector.

15. **Institutional review board (IRB) approvals or equivalent for research with human subjects**

    Question: Does the paper describe potential risks incurred by study participants, whether such risks were disclosed to the subjects, and whether Institutional Review Board (IRB) approvals (or an equivalent approval/review based on the requirements of your country or institution) were obtained?

    Answer: [NA]

    Justification: Our paper does not involve crowdsourcing nor research with human subjects.

    Guidelines:

    - The answer NA means that the paper does not involve crowdsourcing nor research with human subjects.
    - Depending on the country in which research is conducted, IRB approval (or equivalent) may be required for any human subjects research. If you obtained IRB approval, you should clearly state this in the paper.

- We recognize that the procedures for this may vary significantly between institutions and locations, and we expect authors to adhere to the NeurIPS Code of Ethics and the guidelines for their institution.
- For initial submissions, do not include any information that would break anonymity (if applicable), such as the institution conducting the review.

16. **Declaration of LLM usage**

    Question: Does the paper describe the usage of LLMs if it is an important, original, or non-standard component of the core methods in this research? Note that if the LLM is used only for writing, editing, or formatting purposes and does not impact the core methodology, scientific rigorousness, or originality of the research, declaration is not required.

    Answer: [NA]

    Justification: We do not use LLMs for the core method development.

    Guidelines:

    - The answer NA means that the core method development in this research does not involve LLMs as any important, original, or non-standard components.
    - Please refer to our LLM policy (`https://neurips.cc/Conferences/2025/LLM`) for what should or should not be described.

A Prompts Design

We show our prompt design for the multimodal time series forecasting, taking one instance of Typhoon Yutu as an example.

System Prompt & Task Instruction

You are a typhoon forecasting expert. Below are the past 12 hours of typhoon data and the corresponding satellite images. Your task is to forecast the hourly data of the typhoon for the next 12 hours, providing the forecast latitude, longitude, pressure in the same format as the past data format.

Past Data

The corresponding satellite images are: <image> <image> <image> <image> <image> <image> <image> <image> <image> <image> <image> <image>. The historical hourly data from 2018-10-23 01:00:00 to 2018-10-23 12:00:00 is {latitude: [11.65, 11.7, 11.75, 11.8, 11.85, 11.9, 11.95, 11.99, 12.04, 12.09, 12.14, 12.2], longitude: [151.61, 151.41, 151.2, 150.99, 150.79, 150.6, 150.42, 150.26, 150.11, 149.97, 149.83, 149.7], pressure: [974.2, 973.3, 972.5, 971.7, 970.8, 970.0, 967.5, 965.0, 962.5, 960.0, 957.5, 955.0]}.

Label Data

The forecast hourly data is: {latitude: [12.26, 12.34, 12.42, 12.5, 12.6, 12.7, 12.81, 12.93, 13.05, 13.17, 13.29, 13.4], longitude: [149.57, 149.44, 149.31, 149.18, 149.04, 148.9, 148.76, 148.61, 148.46, 148.31, 148.15, 148.0], pressure: [954.2, 953.3, 952.5, 951.7, 950.8, 950.0, 945.8, 941.7, 937.5, 933.3, 929.2, 925.0].}

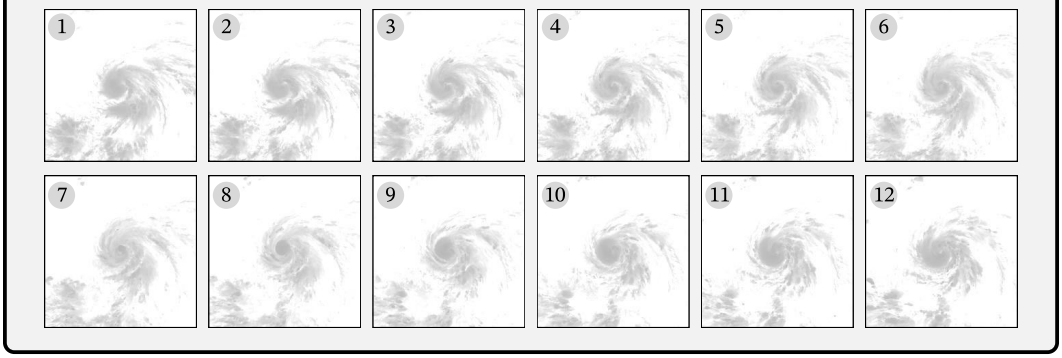

B Method

B.1 Algorithms

In this section, we present the algorithms for PIPE (algorithm 1), which integrates physical information into VLMs. To begin, we extract the required physical information (algorithm 2) from the time series data corresponding to each satellite image. This information includes the timestamp and geocoordinates for the typhoon's eye. Additionally, since satellite images are divided into patches, we calculate the geocoordinates for the center of each patch. Next, we incorporate this physical information into the positional encoding of VLMs through physics-informed positional indexing (algorithm 3). Beyond indexing, we adapt the sinusoidal function by introducing variant-frequency sinusoidal encoding (algorithm 4), which embeds the frequency attributes of the variables into the positional embedding. This enhanced positional embedding is then added to the input embedding of the corresponding image tokens. Finally, these integrations are utilized to predict the next token, enabling the model to leverage both spatial and physical context effectively.

Algorithm 1: PIPE

Require: Time series input $\boldsymbol{x}$, corresponding image $\boldsymbol{i}$
Ensure: Next token prediction $\boldsymbol{T}_{next}$

$\boldsymbol{T}_{text}, \boldsymbol{T}_{image}$ = tokenizer($\boldsymbol{x}$), vision_encoder($\boldsymbol{i}$) ▷ Tokenization
$\boldsymbol{t}, \boldsymbol{lat}, \boldsymbol{lng} \leftarrow$ get_physic($\boldsymbol{x}, \boldsymbol{T}_{image}$) ▷ Extract physical info (algorithm 2): $\boldsymbol{t}, \boldsymbol{lat}, \boldsymbol{lng} \in \mathbb{R}^{1 \times len(\boldsymbol{T}_{image})}$
$\boldsymbol{ids} \leftarrow$ position_indexing($\boldsymbol{T}_{text}, \boldsymbol{T}_{image}, \boldsymbol{t}, \boldsymbol{lat}, \boldsymbol{lng}$) ▷ Compute physics-informed indices (algorithm 3): $\boldsymbol{ids} \in \mathbb{R}^{3 \times len(\boldsymbol{T}_{text}+\boldsymbol{T}_{image})}$)
$\boldsymbol{PE} \leftarrow$ vf_fun($\boldsymbol{pos}, \boldsymbol{i}$) ▷ Generate variant-frequency position embedding (algorithm 4): $\boldsymbol{PE} \in \mathbb{R}^{len(\boldsymbol{T}_{text}+\boldsymbol{T}_{image}) \times d_{model}}$
$\boldsymbol{IE} \leftarrow [\boldsymbol{T}_{text}, \boldsymbol{T}_{image}] \oplus \boldsymbol{PE}/d_{model}$ ▷ Update input embeddings
$\boldsymbol{T}_{next} \leftarrow f_{VLM}(\boldsymbol{IE}, \boldsymbol{ids})$ ▷ Predict next token

Algorithm 2: Extract Physical Information for Image Tokens

Require: Input $\boldsymbol{x}, \boldsymbol{T}_{image}$
Ensure: Time ($\boldsymbol{t}_{day}, \boldsymbol{t}_{hour}$) and location ($\boldsymbol{lat}, \boldsymbol{lng}$) for each image tokens

$\boldsymbol{t} \leftarrow \boldsymbol{x}$ ▷ Extract temporal information from time series input (Equation 7)
$\boldsymbol{t}_{day}, \boldsymbol{t}_{hour} \leftarrow \boldsymbol{t}//24, \boldsymbol{t}\%24$
$\boldsymbol{lat}_{image}, \boldsymbol{lng}_{image} \leftarrow \boldsymbol{x}$ ▷ Extract spatial information for the entire image.
$\boldsymbol{lat}, \boldsymbol{lng} \leftarrow$ get_center($\boldsymbol{T}_{image}, \boldsymbol{lat}_{image}, \boldsymbol{lng}_{image}$) ▷ Compute center coordinates for patches

Algorithm 3: Physics-Informed Positional Indexing

Require: $\boldsymbol{T}_{text}, \boldsymbol{T}_{image}, \boldsymbol{t}, \boldsymbol{lat}, \boldsymbol{lng}$
Ensure: Physics-Informed $\boldsymbol{ids}$
1: $\boldsymbol{ids}_{text} \leftarrow$ sequential_indexing ▷ Assign sequential indices to text tokens (Equation 5)
2: $\boldsymbol{ids}_{image} \leftarrow$ physics-informed indexing ▷ Assign $[\boldsymbol{t}, \boldsymbol{lat}, \boldsymbol{lng}]$ to image tokens (Figure 2)
3: $\boldsymbol{ids} \leftarrow [\boldsymbol{ids}_{text}, \boldsymbol{ids}_{image}]$ ▷ $\boldsymbol{ids} \in \mathbb{R}^{3\times len(\boldsymbol{T}_{text}+\boldsymbol{T}_{image})}$)

Algorithm 4: Variant-Frequency Sinusoidal Encoding

Require: Position $\boldsymbol{pos}$
Ensure: Variant-frequency position embedding $\boldsymbol{PE}$
1: $\boldsymbol{PE}_{text} \leftarrow$ standard sinusoidal function (Equation 1)
2: $\boldsymbol{PE}_{image} \leftarrow$ variant-frequency sinusoidal function (Equation 9)
3: $\boldsymbol{PE} \leftarrow [\boldsymbol{PE}_{text}, \boldsymbol{PE}_{image}]$

B.2 Variant-frequency sinusoidal function

This section presents the complete formal definition of the variant-frequency sinusoidal function. The model dimensions are partitioned into two distinct components: temporal dimensions (first half) and spatial dimensions (latter half). Regarding the temporal dimensions, they combine the encoding of t_{day} and t_{hour}. Similarly, for the spatial dimensions, they combine the latitude embeddings for lat and the longitude embeddings for lng. This dimensional combination enables simultaneous representation of both temporal and spatial characteristics within the unified model framework. We also visualize the function (Figure 4) taking the $d_{model} = 128$ as an example.

$$
\begin{aligned}
PE_{(pos,4i)} &= sin(\frac{t_{day}}{10000^{4i/d_{model}}} \times \frac{2\pi}{p_{day}})\ if\ 4i \leq \frac{d_{model}}{2} \\
PE_{(pos,4i+1)} &= cos(\frac{t_{day}}{10000^{4i/d_{model}}} \times \frac{2\pi}{p_{day}})\ if\ 4i+1 \leq \frac{d_{model}}{2} \\
PE_{(pos,4i+2)} &= sin(\frac{t_{hour}}{10000^{4i/d_{model}}} \times \frac{2\pi}{p_{hour}})\ if\ 4i+2 \leq \frac{d_{model}}{2} \\
PE_{(pos,4i+3)} &= cos(\frac{t_{hour}}{10000^{4i/d_{model}}} \times \frac{2\pi}{p_{hour}})\ if\ 4i+3 \leq \frac{d_{model}}{2} \\
PE_{(pos,4i)} &= sin(\frac{lat}{10000^{4i/d_{model}-1/2}} \times \frac{2\pi}{p_{lat}})\ if\ \frac{d_{model}}{2} < 4i \leq d_{model} \\
PE_{(pos,4i+1)} &= cos(\frac{lat}{10000^{4i/d_{model}-1/2}} \times \frac{2\pi}{p_{lat}})\ if\ \frac{d_{model}}{2} < 4i+1 \leq d_{model} \\
PE_{(pos,4i+2)} &= sin(\frac{lng}{10000^{4i/d_{model}-1/2}} \times \frac{2\pi}{p_{lng}})\ if\ \frac{d_{model}}{2} < 4i+2 \leq d_{model} \\
PE_{(pos,4i+3)} &= cos(\frac{lng}{10000^{4i/d_{model}-1/2}} \times \frac{2\pi}{p_{hour}})\ if\ \frac{d_{model}}{2} < 4i+3 \leq d_{model}
\end{aligned}
\tag{9}
$$

where for temporal dimensions $p_{day} = 366$ and $p_{hour} = 24$, while for spatial dimensions, $p_{latitude} = 180$ and $p_{longitude} = 360$. t_{day} is the day of the year (ranging from 0 to 365) and t_{hour} represents the hour of the day (ranging from 0 to 23). lat is the latitude of the image token, and lng is the longitude of the image token.

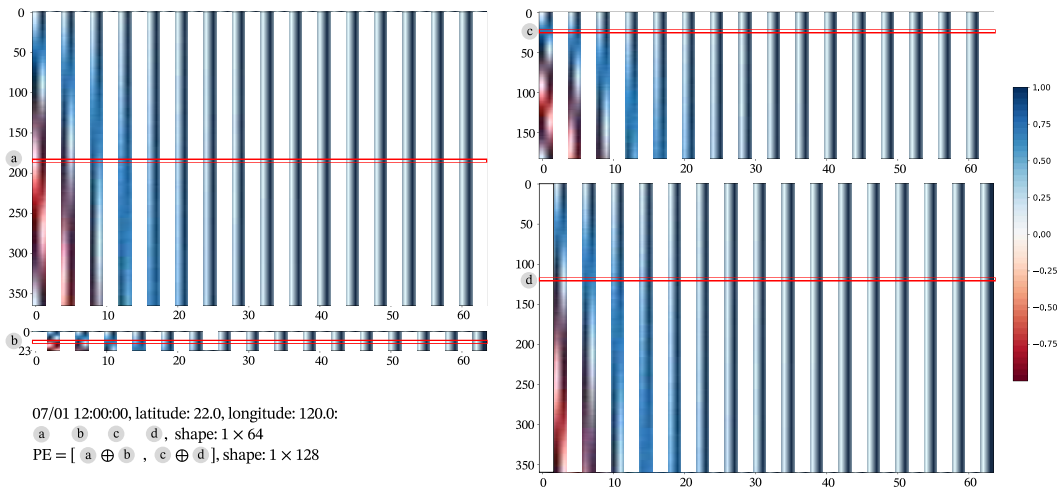

Figure 4: The 64-dimensional positional encoding for the physical variables. Each row represents the embedding vector. The final position encoding will be 128-dimensional by combining them.

C Implementation Details

VLMs training We leverage LLama-Factory [60] for training VLMs, utilizing PyTorch [38] on NVIDIA H800 GPUs. The optimization process employs the AdamW optimizer [33] with an initial learning rate of 10^{-5} (using the cosine scheduler), a batch size of 1, and CrossEntropy loss over 1 training epoch. We provide the code for the reproduction.

Non-vision models One Fits All [62] and AutoTimes [32] are implemented using their official repositories, adapted to accommodate our typhoon sequence dataset via modifications to the data loader. Configuration follows original specifications: model dimensions of 768 (One Fits All) and 512 (AutoTimes), with a batch size of 128, learning rate of 10^{-4}, and 10 training epochs. For other AI models, we use the publicly available platform Time-Series-Library [56] to implement them. The parameters for model dimensions and number of heads are based on their implementation (512) with a batch size of 128 and a learning rate of 10^{-4}, training epochs of 30, and patience of 10.

For domain models, the results are provided by the original paper.

Training Cost We use 4×NVIDIA H800 GPUs to train the models for one epoch. The training time varies significantly across model sizes:

- PIPE-3B: 2.1 hours
- PIPE-7B: 3.7 hours
- PIPE-32B (LoRA [14] rank as 8): 0.7 hours

The PIPE-32B variant achieves substantial time efficiency through LoRA, which reduces trainable parameters while maintaining competitive performance (as shown in Tables 9 and 10). This demonstrates an effective balance between model capacity and computational overhead. For baseline AI models (including LLM-based variants like AutoTimes (OPT model)), training completes in 1 hour with a single NVIDIA RTX 4090 GPU.

D Dataset

We provide a comprehensive summary of the Digital Typhoon dataset [22].

Table 4: The detailed information of the Digital Typhoon dataset.

	Digital Typhoon dataset
Temporal coverage	1978-2023 (present)
Temporal resolution	one hour
Target satellites	Himawari
Spatial coverage	Western North Pacific basin
Spatial resolution	5km
Image coverage	512×512 pixels (1250km from the center)
Spectral coverage	infrared (others on the Website)
Map projection	Azimuthal equal-area projection
Calibration	Recalibration
Data format	HDF5
Best track	Japan Meteorological Agency
Dataset browsing	Digital Typhoon website

Table 5: Multimodal time series forecasting results (leading time is 12h).

	Models	Intensity (hPa) MAE	Intensity (hPa) RMSE	Latitude (°) MAE	Latitude (°) RMSE	Longitude (°) MAE	Longitude (°) RMSE	Distance (km) MAE
domain	ECMWF-HRES [10]	\	\	\	\	\	\	44.972
	PanGu [3]							<u>44.630</u>
	GenCast [40]							**37.930**
	TIFS [35]	\	9.061					\
w/o vision	PatchTST [34]	<u>3.917</u>	**5.989**	0.465	0.615	0.751	0.931	103.818
	iTransformer [31]	4.004	<u>6.157</u>	0.412	0.558	0.565	0.736	83.174
	Crossformer [51]	4.257	6.303	0.546	0.726	0.844	1.109	118.748
	TimeXer [53])	5.380	7.911	0.563	0.755	0.713	0.962	108.665
	TiDE [9]	3.926	6.080	0.416	0.561	0.677	0.850	93.570
	One Fits All [62])	4.039	6.212	0.420	0.568	0.586	0.759	85.555
	AutoTimes [32]	4.086	6.220	0.448	0.600	0.692	0.872	97.244
	TimesNet [55]	4.798	7.220	0.892	1.133	1.796	2.147	230.376
	TimeMixer [50]	4.227	6.290	0.400	<u>0.533</u>	0.524	0.685	78.569
vision	Original paper [22]	\	12.100	\	\	\	\	\
	Qwen-2.5-VL-3B [2]	3.963	6.599	<u>0.371</u>	0.535	<u>0.435</u>	<u>0.610</u>	69.959
	PIPE-3B	**3.855**	6.333	**0.359**	**0.526**	**0.411**	**0.587**	67.114

E Supplementary Results

E.1 Forecasting Results of More Leading Times

We present additional forecasting analyses in this section. First, we list the 12-hour lead-time forecasting performance of all baseline models (Table 5). Our model demonstrates state-of-the-art results across the majority of the evaluation metrics. Second, we list the result of the ablation study when the leading time is 12 hours. The consistency between results at different leading times confirms the robustness of our architectural design, demonstrating that all modules contribute meaningfully to forecasting accuracy. Finally, we visualize the MAE for the forecasting of pressure, latitude, longitude, and distance across lead times ranging from 1 to 12 hours (Figure 5). The results confirm that our model consistently achieves the lowest MAE values at all forecast leading times. This systematic advantage over baseline models highlights the effectiveness of our model in maintaining forecasting precision as the leading time increases.

Table 6: The results of the ablation study (leading time is 12h).

Models	Intensity (hPa) MAE	Intensity (hPa) RMSE	Latitude (°) MAE	Latitude (°) RMSE	Longitude (°) MAE	Longitude (°) RMSE	Distance (km) MAE
w/o vision	4.120	6.820	0.372	0.532	0.436	0.616	70.138
w/o 3D indexing (using sequence)	3.936	6.809	0.366	0.535	0.434	0.611	69.382
w/o physics-informed indexing (using 3D)	3.963	6.599	0.371	0.535	0.435	0.610	69.959
w/o negative indexing	4.282	7.017	0.550	0.806	0.869	1.306	124.329
w/o entire sinusoidal function	**3.827**	6.387	0.364	0.527	0.416	0.590	67.904
w/o variant-frequency sinusoidal function	4.071	6.689	0.370	0.537	0.429	0.604	69.389
PIPE-3B	3.855	**6.333**	**0.359**	**0.526**	**0.411**	**0.587**	**67.114**

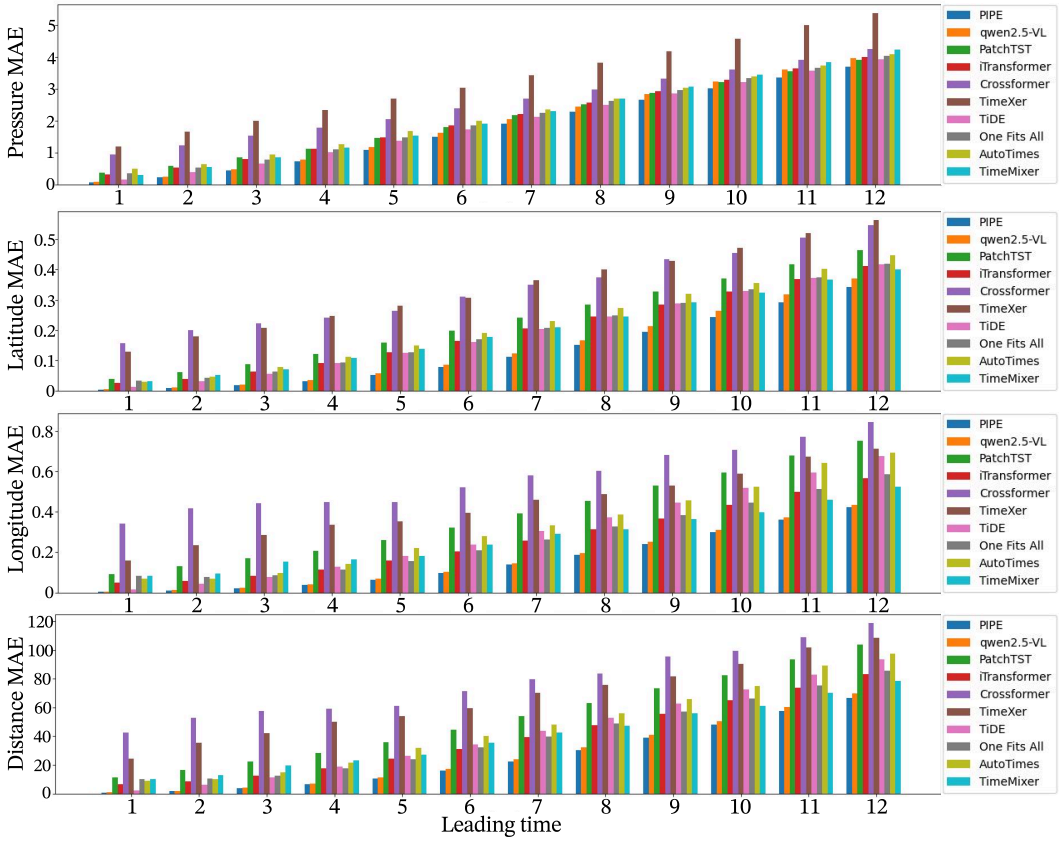

Figure 5: The performance across leading times ranging from 1 to 12 hours.

E.2 Experiment Statistical Report

The stability of PIPE's forecasting performance is validated through standard deviation analysis across three random seeds, reported in Tables Table 7 and Table 8.

E.3 Scaling Behavior

To evaluate the impact of model size on performance, we conduct experiments across three variants: PIPE-3B, PIPE-7B, and PIPE-32B (with LoRA rank as 8). As demonstrated in Tables 9 and 10, the largest model, PIPE-32B, yields performance improvements, even when leveraging LoRA.

Table 7: The mean and the standard deviation of PIPE-3B from three random seeds (leading time is 6 hours).

Models	Intensity (hPa)		Latitude (°)		Longitude (°)		Distance (km)
	MAE	RMSE	MAE	RMSE	MAE	RMSE	MAE
PIPE-3B-seed1	1.503	2.940	0.085	0.161	0.095	0.178	16.364
PIPE-3B-seed2	1.513	2.946	0.082	0.154	0.094	0.173	16.000
PIPE-3B-seed3	1.529	3.059	0.084	0.161	0.097	0.181	16.463
PIPE-3B	1.515 ± 0.011	2.981 ± 0.055	0.084 ± 0.001	0.159 ± 0.003	0.095 ± 0.001	0.178 ± 0.003	16.275 ± 0.200

Table 8: The mean and the standard deviation of PIPE-3B from three random seeds (leading time is 12 hours).

Models	Intensity (hPa)		Latitude (°)		Longitude (°)		Distance (km)
	MAE	RMSE	MAE	RMSE	MAE	RMSE	MAE
PIPE-3B-seed1	3.840	6.295	0.362	0.530	0.412	0.590	67.432
PIPE-3B-seed2	3.831	6.281	0.355	0.523	0.405	0.578	66.402
PIPE-3B-seed3	3.893	6.425	0.360	0.527	0.415	0.592	67.506
PIPE-3B	3.855 ± 0.027	6.333 ± 0.065	0.359 ± 0.003	0.526 ± 0.003	0.411 ± 0.004	0.587 ± 0.006	67.114 ± 0.050

Table 9: The results of PIPE-3B, PIPE-7B, and PIPE-32B (with LoRA) with the lead time of 6 hours.

Models	Intensity (hPa)		Latitude (°)		Longitude (°)		Distance (km)
	MAE	RMSE	MAE	RMSE	MAE	RMSE	MAE
PIPE-3B	1.515	2.981	0.084	0.159	0.095	0.178	16.275
PIPE-7B	1.505	2.918	0.088	0.166	0.102	0.184	17.194
PIPE-32B	1.505	2.874	0.079	0.153	0.097	0.182	15.980

E.4 Forecasting Results on Different Grades

We experiment to investigate the performance of our method on different grades of typhoons. We split the dataset based on the grade (from grade 2 to grade 6). Grade 2 represents tropical depressions, which are weaker cyclones and not classified as tropical cyclones. Grades 3, 4, and 5 represent tropical cyclones, with Grade 5 being the most intense. Grade 6 represents a cyclone with a different structural system from tropical cyclones. Then we train models on different sub-datasets. The results are shown in Table 11.

Track Forecasting vs. Pressure Forecasting Tropical cyclones (Grades 3, 4, 5) demonstrate better track forecasting performance compared to non-tropical cyclones (Grades 2, 6). This is likely due to the more stable and predictable system of tropical cyclones, which facilitates track forecasting. However, pressure forecasting is more challenging for tropical cyclones due to higher variability and complexity. In contrast, non-tropical cyclones (Grade 2 and Grade 6) exhibit more predictable pressure patterns but greater difficulty in track forecasting. This is especially pronounced before the cyclone structure forms (Grade 2) and after it breaks (Grade 6).

Impact of Intensity on Forecasting As the intensity of tropical cyclones increases (Grades 3, 4, 5), pressure forecasting becomes progressively more challenging. However, the difficulty of track forecasting remains relatively consistent across these grades.

Impact of Data Volume Models trained on all grades perform better in track forecasting compared to models trained on individual grades. This result indicates that a larger volume of training data improves track forecasting accuracy across different cyclone intensities.

E.5 Experiment on the Offset Indexing

In addition to negative indexing, we investigate an alternative approach called offset indexing, where all image tokens are assigned an offset equal to the maximum length of the textual tokens to address conflicts between the physical information of vision tokens and the order information of text tokens.

Table 10: The results of PIPE-3B, PIPE-7B, and PIPE-32B (with LoRA) with the leading time of 12 hours.

Models	Intensity (hPa)		Latitude (°)		Longitude (°)		Distance (km)
	MAE	RMSE	MAE	RMSE	MAE	RMSE	MAE
PIPE-3B	3.855	6.333	0.359	0.526	0.411	0.587	67.114
PIPE-7B	3.861	6.325	0.371	0.540	0.435	0.609	69.933
PIPE-32B	3.695	6.029	0.342	0.510	0.423	0.610	66.725

Table 11: The results of the experiment across different grades with the lead time of 6 hours.

Models	Intensity (hPa)		Latitude (°)		Longitude (°)		Distance (km)
	MAE	RMSE	MAE	RMSE	MAE	RMSE	MAE
Grade 2	0.722	1.227	0.108	0.206	0.138	0.245	22.029
Grade 3	0.997	1.772	0.097	0.169	0.115	0.200	18.902
Grade 4	1.656	2.732	0.099	0.156	0.122	0.188	19.310
Grade 5	2.707	4.556	0.090	0.163	0.116	0.203	18.418
Grade 6	1.074	1.830	0.208	0.385	0.283	0.488	37.193

The results of this experiment are presented in Table 12. We find that although offset indexing offers some performance improvement, it falls short compared to PIPE. Our choice of negative indexing remains an intuitive and efficient method for effectively separating different types of tokens.

E.6 Showcase

We present a prediction showcase (Figure 6) to compare our method with the methods that remove satellite imagery and PIPE on the Typhoon Phanfone. PIPE achieves more accurate track forecasting and intensity forecasting.

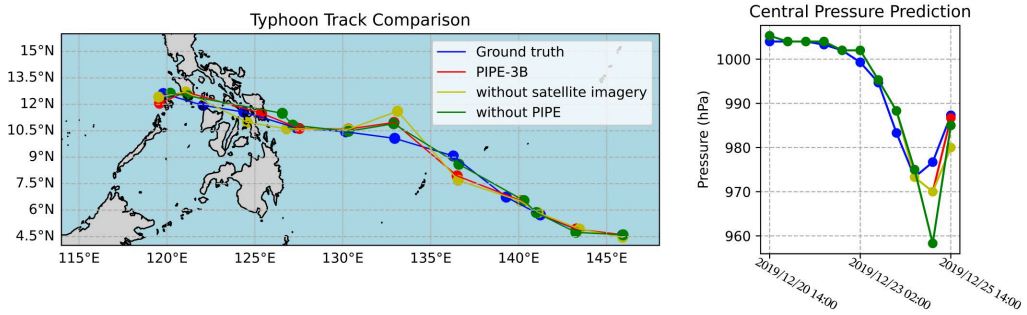

Figure 6: The results of Typhoon Phanfone comparison between PIPE, removing satellite images, and removing PIPE. The leading time is 12 hours and the time gap between neighbouring dots is 12 hours.

E.7 Attention Analysis

We compare the attention from the penultimate layer (Figure 7) with averaging across the head dimension of PIPE-3B and Qwen2.5-VL-3B. It reveals distinct attention patterns. Qwen2.5-VL-3B exhibits an obvious bias toward the initial tokens of the historical time series, as evidenced by an obvious vertical line at 800th input tokens ((e) & (f)). In contrast, our PIPE model allocates greater attention to both the image tokens and the historical time series tokens. Notably, PIPE's attention on image patches is concentrated on the typhoon region (e.g., central cloud structure), whereas

Table 12: The results of offset indexing.

Models	Intensity (hPa)		Latitude (°)		Longitude (°)		Distance (km)
	MAE	RMSE	MAE	RMSE	MAE	RMSE	MAE
no-indexing	1.961	3.926	0.206	0.360	0.388	0.674	53.548
offset indexing	1.815	3.762	0.188	0.303	0.229	0.385	30.157
negative indexing (PIPE)	1.515	2.981	0.084	0.159	0.095	0.178	16.275

Qwen2.5-VL-3B's attention appears diffuse and unstructured across the image. These differences in attention mechanisms likely contribute to PIPE's better forecasting accuracy.

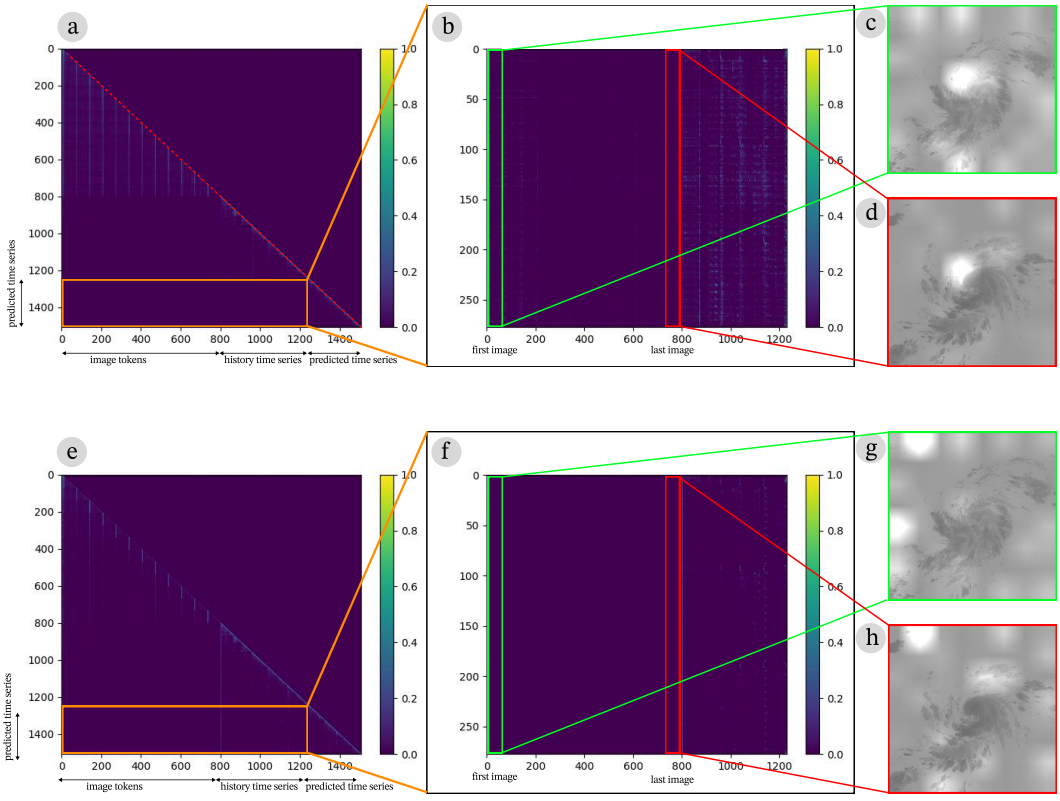

Figure 7: Visualization of attention (normalized to 0-1 in each step) from the penultimate layer of the PIPE model (top) and the Qwen2.5-VL-3B model (bottom), averaged across attention heads. (a) & (e) The entire attention matrix. (b) & (f) The attention matrix of predicted tokens' attention on the input tokens, including image tokens and history time series tokens. (c) & (g) Attention of predicted tokens on the first input image. (d) & (h) Attention of predicted tokens on the last input image.

We also compare the attention using Attention Rollout [1] (Figure 8) with averaging across the head dimension of PIPE-3B and Qwen2.5-VL-3B. It also demonstrates that our model allocates more reasonable attention to image tokens and historical time series tokens. Furthermore, our model's attention on image patches is focused specifically on the typhoon region, whereas Qwen2.5-VL-3B's attention appears biased across the image.

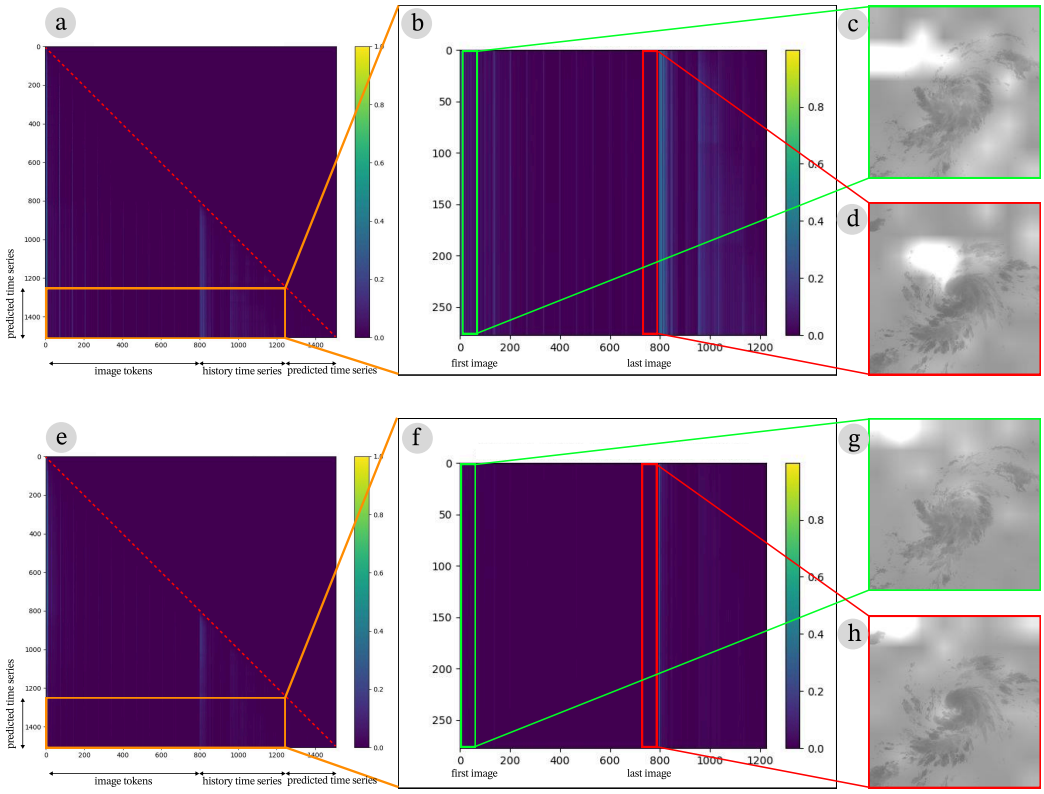

Figure 8: Visualization of attention (normalized to 0-1 in each step) using Attention Rollout of the PIPE model (top) and the Qwen2.5-VL-3B model (bottom), averaged across attention heads. (a) & (e) The entire attention matrix. (b) & (f) The attention matrix of predicted tokens' attention on the input tokens, including image tokens and history time series tokens. (c) & (g) Attention of predicted tokens on the first input image. (d) & (h) Attention of predicted tokens on the last input image.

F Broader Impact

We introduce a novel multimodal time series forecasting task that integrates satellite imagery with temporal data for capturing complex spatio-temporal dependencies. This approach leverages the complementary strengths of temporal time series data and spatially rich visual inputs, enabling models to go beyond the limitations of traditional univariate, multivariate, or single-modality methods. To address the inherent challenges of integrating satellite imagery into time series forecasting, we propose a physics-informed positional encoding. This technique incorporates physical information derived from satellite data, such as geospatial coordinates, to enhance the model's ability to reason about spatial and temporal dependencies. This innovation is particularly relevant for applications where visual inputs carry critical physical context, including climate modeling, urban planning, and agricultural forecasting. The broader impact of this work lies in its ability to bridge the gap between traditional forecasting methods and real-world complexities that often include spatial and physical components. By incorporating satellite imagery and physics-informed encoding, this method has potential benefits across a wide range of scientific and practical domains.